Vertical Structure and Microphysics Analysis from Events of Heavy Rainfall in Brazil

Eliana Cristine Gatti *, Izabelly Carvalho da Costa , Daniel Vila

Posted Date: 15 April 2024

doi: 10.20944/preprints202404.0970.v1

Keywords: heavy rainfall; Weather radars; Nowcasting

 doi:10.20944/preprints202404.0970.v1

Article

Vertical Structure and Microphysics Analysis from Events of Heavy Rainfall in Brazil

Eliana Cristine Gatti [1,*], Izabelly Carvalho da Costa [2] and Daniel Vila [3]

[1] Climatempo, São José dos Campos 122247-016, SP, Brazil; eligatti12@gmail.com
[2] National Institute for Space Research (INPE), Cachoeira Paulista 12630-000, SP, Brazil; izabelly.costa@inpe.br
[2] World Meteorological Organization (WMO): Asuncion, PY; dvila@wmo.int
* Correspondence: eligatti12@gmail.com

Abstract: Intense rainfall events frequently occur in Brazil, often leading to rapid flooding. Despite their recurrence, there is a notable lack of sub-daily studies in the country. This research aims to assess patterns related to the structure and microphysics of clouds driving intense rainfall in Brazil, resulting in high accumulations within 1 hour. Employing a 40 mm/h threshold and validation criteria, 83 events were selected for study, observed by both single and dual-polarization radars. Contoured Frequency by Altitude Diagrams (CFADs) of reflectivity, Vertical Integrated Liquid (VIL), and Vertical Integrated Ice (VII) are employed to scrutinize the vertical cloud characteristics in each region. To address limitations arising from the absence of polarimetric coverage in some events, three case studies focusing on polarimetric variables are included. A fourth case study enhances the overall understanding of these events, emphasizing the underexplored nature of short-term intense rainfall studies in Brazil. Results reveal that the generating system significantly influences the rainfall pattern, especially in the Southern, Southeastern, and Central-Western regions. Regional CFADs unveil primary convective columns with 40-50 dBZ reflectivity, extending to approximately 6 km. The microphysical analysis highlights the rapid structural intensification, challenging the event predictability and the issuance of timely specific warnings.

Keywords: heavy rainfall; Weather radars; Nowcasting

1. Introduction

Brazil is a vast country with a north-south extent of 4394 km. Consequently, its five regions are distributed across a wide range of latitudes, ranging from 5°N to 33°S, and, as a result each region has a distinct climatic regime, as illustrated by [1]. Precipitation is a comum variable utilized to characterize the climate of a region, witch is generated by different meteorological systems that affect each specific area.

A significant portion of precipitating systems that define the pluviometric regime of a region gives rise to episodes of intense rainfall, often considered extreme. However, there is no consensus regarding the definition of the term in the literature, as it varies depending on data availability, study area, and the objectives of each research. For instance, works such as [2–5] use fixed thresholds to characterize episodes of intense rainfall. In Brazil, [6] define for the Southern region of Brazil when the 50 mm isohyet encompasses a minimum area of 10,000 km^2. [7] and [8] define an extreme event when daily precipitation exceeds a certain percentage of the seasonal climatological total for a specific station. Additionally, some authors choose to assess intense rainfall through the use of percentiles, such as [9–11]. This methodology is widely used when identifying precipitation extremes based on typical precipitation patterns in a given region.

Although several methods exist to define it, a significant portion of studies on the subject consider daily-scale precipitation. However, many events associated with flash floods, runoff, and/or rapid inundations occur over a short period. Studies are scarce regarding intense rainfall events on a sub-daily scale in Brazil, and existing studies focus on specific regions, such as [11]. Therefore, there is still a need for a more comprehensive evaluation of events occurring over a short period across the country to identify similar characteristics and possibly enhance predictability.

With the inclusion of meteorological radars, particularly those with dual polarization, the understanding of the microphysical structure of precipitation improves in the absence of in situ mea-

 doi:10.20944/preprints202404.0970.v1

surements and microphysical processes within observed precipitation [12]. This improvement results from the availability of new variables capable of inferring additional parameters compared to single-polarization (conventional) radars [13]. Over the last ten years, Brazil has acquired a network of polarimetric radars covering parts of the country, although the majority are still of the conventional type. Despite limitations in observations of physical cloud processes with conventional radars (though not nonexistent), the country lacks information on the subject, necessitating its inclusion in research.

In this context, the main objective of this study is to investigate the structure and microphysical aspects associated with clouds generating intense rainfall over Brazil, leading to high accumulations in a very short period (1 hour). Thus, the study explores the possibility of any patterns in the clouds that may generate such events. However, it is important to note that this study does not differentiate between synoptic systems responsible for event generation to truly ascertain if there is any similarity between all types of systems. Therefore, this study can be conducted for different regions of Brazil, regardless of the meteorological systems affecting them.

Finally, it is worth highlighting the innovative content in this study. No other works in the country have assessed the structure of intense rainfall events in the very short term using national-level polarimetric radar data. Therefore, a significant portion of the results is limited to comparison and discussion with international literature.

2. Materials and Methods

2.1. Data and Study Area

The data used to identify intense rainfall events are obtained from automatic rain gauges provided by the National Institute of Meteorology (INMET), with a 1-hour frequency spanning from 2016 to 2020, encompassing a total of 5 years of data. Constant Altitude Plan Position Indicator (CAPPI) data from nine S-band polarimetric radars (2-4 GHz) owned by the National Center for Monitoring and Early Warning of Natural Disasters (CEMADEN) are employed. As the polarimetric radar network covers only certain regions of Brazil, additional single-polarization (S-band) radars from two other agencies are incorporated—six from the Department of Airspace Control (DECEA) and four from the Amazon Protection System (SIPAM). Consequently, this study utilizes the study areas limited by the radar coverage distributed across all regions of Brazil (Figure 1). The National Institute for Space Research (INPE) provides the data for each radar. Table 1 presents the 19 radars used for the analyses in this study.

 doi:10.20944/preprints202404.0970.v1

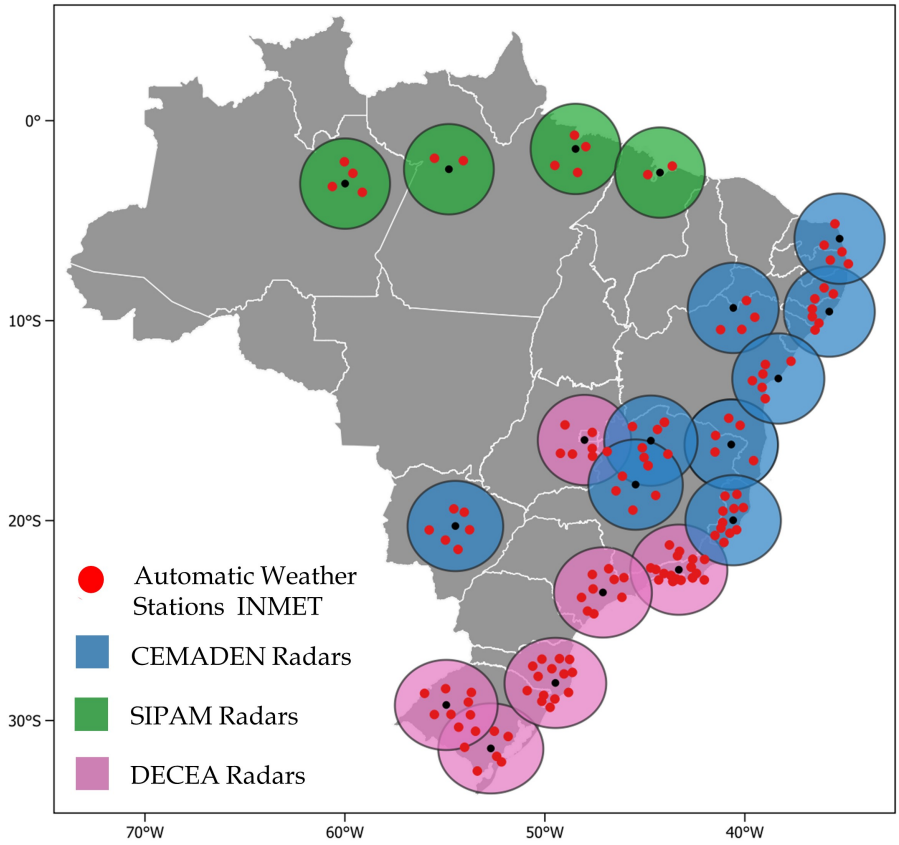

Figure 1. Spatial distribution of CEMADEN, DECEA and SIPAM radars in Brazilian territory, with INMET stations selected for the study.

2.2. Case Selection

2.2.1. Weather Stations

We first applied a filter to choose INMET stations located within the radar domains to select intense rainfall events. To calculate the distance between two points on a sphere based on their geographical coordinates, we use the Haversine formula, represented by Equation 1.

$$D = 2\,R\,arcsin\sqrt{sin^2\left(\frac{\phi_2-\phi_1}{2}\right)+cos(\phi_1)cos(\phi_2)sin^2\left(\frac{\lambda_{lon,2}-\lambda_{lon,1}}{2}\right)} \quad (1)$$

where D is the distance in km, R is the radius of the Earth, ϕ is the latitude and λ_{lon} the longitude.

By calculating the distance between the INMET station locations and the central points of the radars, we identify stations within the coverage area of each radar. Additionally, the stations must be located within a specified distance from the radar centers (which will be defined later). This detail requires consideration because if a station is too close to the radar, it is affected by the blind cone (an area without data), hindering event analysis. Furthermore, as the distance increases, the radar beam becomes higher due to antenna inclination and the curvature of the Earth. If the distance is too large, the lower radar elevation may only capture information from the upper parts of the cloud, neglecting the lower portions, which also hinders analyses. Thus, a distance range is defined to minimize the occurrence of these errors. It is essential to emphasize that such a limitation is necessary as the goal of this study is to assess the complete vertical profile of clouds, not just surface-level precipitation.

 doi:10.20944/preprints202404.0970.v1

Table 1. S-band radars from CEMADEN, DECEA, and SIPAM used for the analyses.

Radar/ OP	UF	Polarization	Frequency
Almenara/ CEMADEN	MG	Dual-polarization	10 min
Jaraguari/ CEMADEN	MS	Dual-polarization	12 min
Maceio/ CEMADEN	AL	Dual-polarization	10 min
Natal/ CEMADEN	RN	Dual-polarization	10 min
Petrolina/ CEMADEN	PE	Dual-polarization	10 min
Salvador/ CEMADEN	BA	Dual-polarization	10 min
Santa Tereza/ CEMADEN	ES	Dual-polarization	10 min
São Francisco/ CEMADEN	MG	Dual-polarization	10 min
Três Marias/ CEMADEN	MG	Dual-polarization	10 min
Canguçu/ DECEA	RS	Single polarization	10 min
Gama/ DECEA	GO	Single polarization	10 min
Morro da Igreja/ DECEA	SC	Single polarization	10 min
Pico do Couto/ DECEA	RJ	Single polarization	10 min
Santiago/ DECEA	RS	Single polarization	12 min
São Roque/ DECEA	SP	Single polarization	10 min
Manaus/ SIPAM	AM	Single polarization	12 min
Santarém/ SIPAM	PA	Single polarization	12 min
São Luiz/ SIPAM	MA	Single polarization	12 min
Belém/ SIPAM	PA	Single polarization	12 min

We select a limit of 150 km from the radar's central point, based on [14], to obtain more accurate data and avoid the previously mentioned issues. For the lower limit, we calculate the height and distance of the beam based on the elevations of each radar used in this study. After performing the procedure for all radars, we found that beyond a distance of 50 km, all are outside the blind cone limits. Thus, we use thresholds between 50 and 150 km to filter the stations. Figure 1 shows the INMET stations that comply with the established thresholds.

2.2.2. Heavy Rain

Various methodologies are used to classify intense rainfall, each with different objectives. The percentile technique is frequently utilized when the goals pertain to differentiating intense rainfall among various regions. However, intense rainfall is often correlated with damages and disturbances caused by such events. When the objective involves the inclusion of such correlations, it is important to acknowledge that other variables need consideration beyond the percentile outcome. For instance, if a certain rainfall rate is deemed high by the percentile but affects a forested area or a city with efficient drainage and water flow, the likelihood of causing damage is reduced. In this study, as the objective is more related to the cloud's capability to generate high-intensity rainfall than distinguishing extremes between regions and correlating with surface damages, a fixed threshold of 40 mm/h is chosen for case selection. This threshold was chosen subjectively, based on the fact that if a cloud produces this amount of rainfall in just one hour, it is considered of high intensity regardless of the region where it occurs.

In this study, we consider "cases" to be all instances where rainfall exceeded the established threshold and "events" as all cases that recorded accumulations within a single hour or with a maximum interval of 2 hours between recordings. We selected 385 cases of intense rainfall across the study area based on the established conditions.

2.3. Cases Validation

We first used radar data to validate the selected cases concerning rainfall records from INMET stations. The validation methodology includes verifying if rainfall was recorded at the station and if

 doi:10.20944/preprints202404.0970.v1

the radar identified rainfall at the same location. Figure 2 illustrates the validation process. Firstly, we created a 5x5 *km* area centered on the station's location. This area is equivalent to 25 km^2, given that the horizontal resolution of the grid interpolated from radar data is 1 *km*. Subsequently, a temporal variation of 1 hour is conducted using radar data to identify if rainfall was indicated at the location. This period was chosen based on how accumulated data is stored over time. For instance, if an INMET station recorded 30 *mm* at 21 UTC, it means that rainfall occurred between 20 and 21 UTC. The entire period is analyzed as the exact rainfall time within this 1 hour is unknown. Since radars have a frequency of 10 or 12 minutes, 6 or 5 images are evaluated within the period respectively (t+5 or t+4, Figure 2). If any pixel within the 5x5 *km* area records a reflectivity greater than or equal to 40 *dBZ* sometime during the analyzed period, the case remains selected for further checks. Additionally, among all times analyzed within the hour, the one that recorded the pixel with the highest reflectivity value in the 5x5 *km* area over the station is considered the time of registration of the maximum pixel value, hereafter referred to as PMAX. We chose this methodology of the area centered on the station because there may be some displacement between the exact station point and the radar information due to the Earth's curvature.

We excluded 196 cases after the rain accumulation validation stage for reasons of not reaching the predicted reflectivity limits or for presenting missing radar data during the analyzed period. Cases with missing data were excluded, mainly due to the frequency of radar data. With the same variations of 10 to 12 minutes, if a piece of data is missing, a gap of 20 minutes without data is observed, which significantly impairs the analyses performed.

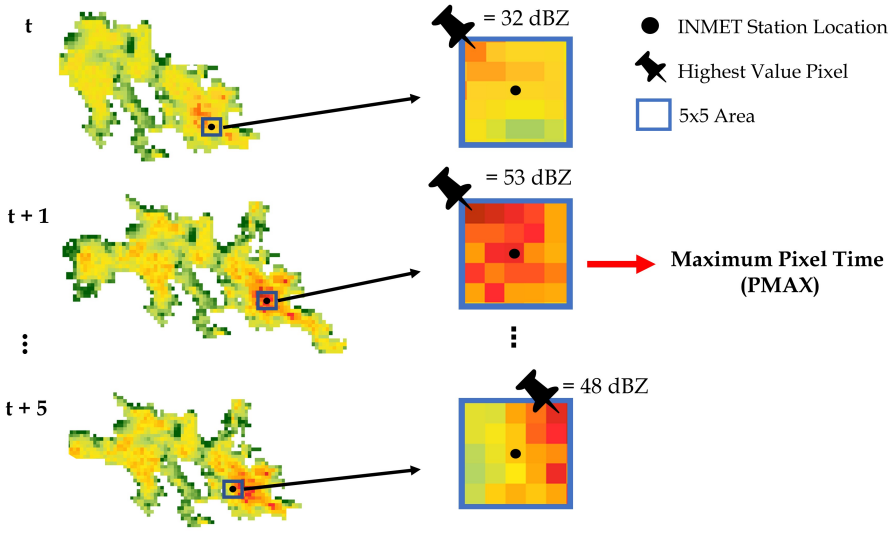

Figure 2. Example of case's validations. For each time analysis, an area 5x5 *km* is created centered on the same station coordinate, and the time of the pixel with the highest value (PMAX) is recorded.

2.4. Vertical Structure and Microphysical Processes

The radar data used was made available by INPE in HDF5 and vol. We converted the data to cartesian coordinates to facilitate manipulation and visualization using the CAPPI projection from 2 to 16 *km*, using the TRMM Radar Software Library (RSL) and saved in NetCDF format.

To compare events occurring in different regions of Brazil, we conducted analyses of the vertical structure of storms using the CFAD methodology and calculating VIL and VII, which will be further discussed in the following sections. Since dual-polarization radars provide additional variables compared to single-polarization radars, the analyses encompassing the regions of Brazil as a whole are limited to the reflectivity variable, as it is a common variable between conventional and polarimetric

 doi:10.20944/preprints202404.0970.v1

radars. However, to evaluate the microphysics of storms in more detail, 4 case studies are added. Below, we explain the methodologies and processes used to develop each analysis separately.

2.4.1. Traking

To begin the analysis, we first tracked the pre-selected and validated cases. For this purpose, the TATHU software (Tracking and Analysis of Thunderstorms) [15], provided and operationally used by INPE, was employed. TATHU is a program developed in the Python language for tracking convective systems, initially using satellite and/or meteorological radar data. The radar module utilizes reflectivity data (in this study, the 3 km CAPPI) to track storm cores over time. Using a threshold of 35 dBZ [16], which can be adjusted based on each research objective, TATHU creates a contour around the cores with reflectivity equal to or greater than the chosen threshold. By adding a temporal series of radar data, TATHU identifies cores in each dataset, enabling the tracking of storm movement over time. In situations where a division of the tracked core occurs, TATHU follows the one displaying greater intensity. In addition, for each tracked core, a unique code is generated. As time varies, the program recognizes the same core from the previous image, and the code remains the same at each time step. Thus, by identifying the code of the storm in question, the tracking of the specific event responsible for generating each intense rainfall event is obtained.

The analyses aim to assess cloud evolution in moments before and after rainfall. Since intense rainfall records are hourly, they encompass rainfall that occurred in the previous hour. For example, if the station recorded rainfall > 40 mm at 18 UTC, it occurred between 17 and 18 UTC. As the desire is to evaluate moments before and after, the temporal period added to TATHU was selected as 2 hours before and 1 hour after the recording time of each case. Thus, within this interval, the cloud's lifetime is limited.

With the information about the position of each station in INMET, it was possible to determine which core, tracked by TATHU, was responsible for generating the intense rainfall event. After that, we extracted the georeferenced shapefile of the core's contour for each time step of the cloud's life cycle for all selected cases (Figure 3).

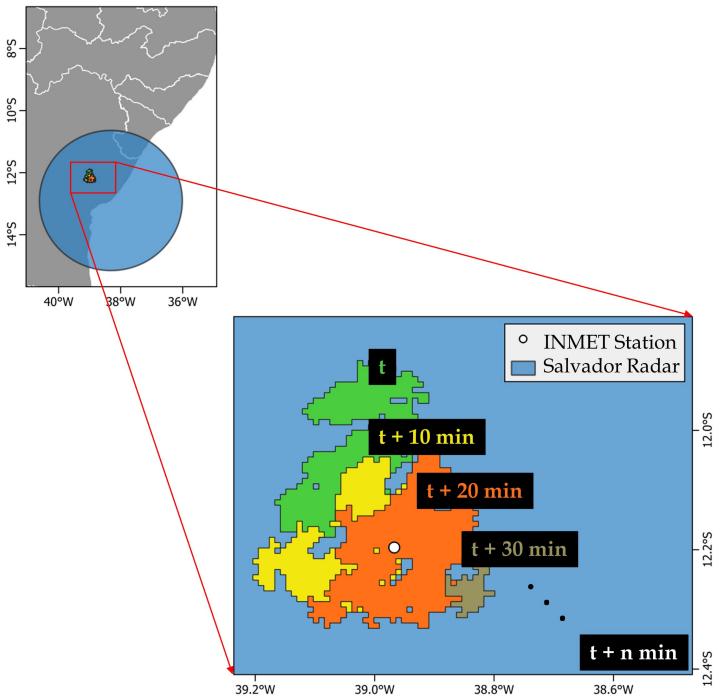

Figure 3. Exemplification of the tracking carried out for a case that occurred in the municipality of Feira de Santana - BA, which is covered by the Salvador radar. The colors indicate the shapefile extracted at each time step of the storm.

 doi:10.20944/preprints202404.0970.v1

2.4.2. VIL and VII

Single-polarization radars have a limited number of variables compared to polarimetric radars. However, Brazil still has a relatively small network of polarimetric radars compared to conventional ones, which motivates their use in this study. Since two types of radars are employed, different methodologies are applied to calculate the water and ice content within the cloud, as outlined below.

For single-polarization radars, the integrated liquid water content, VIL, is calculated based on [17]. VIL represents the relationship between liquid water content and radar reflectivity and is computed along the vertical column using Equation 2.

$$VIL(Z) = 3,4 \times 10^{-6} \int_{h_{base}}^{h_{top}} Z^{4/7} \cdot dh \quad [kg/m^2] \tag{2}$$

where, Z is the reflectivity factor ($mm^6 m^{-3}$), h_{base} and h_{top} are, respectively, the height (meters) of the base and the top of the precipitation column (i.e., $Z \geq 0$ dBZ).

VII (Vertically Integrated Ice), as discussed in [18], is calculated using the Equation 3:

$$VII(Z) = 6,07 \times 10^{-3} \int_{h_{-10°C}}^{h_{-40°C}} Z^{4/7} \cdot dh \quad [kg/m^2] \tag{3}$$

where, Z is the reflectivity factor ($mm^6 m^{-3}$), $h_{-10°C}$ and $h_{-40°C}$ are the heights of the isotherms of -10 °C and -40 °C, respectively, which are obtained from the soundings closest to the location of each radar.

Vertical integration is limited to the thermodynamic layer between -10 and -40 °C, which is the ice growth layer within a storm [19].

Calculations related to water content can lead to errors when using classical relationships [60]. In the case of polarimetric radars, equations using polarimetric variables are utilized, which studies confirm as more efficient than classical relationships [20–25]. Therefore, in this study, for cases covered by polarimetric radars, VIL is calculated through the integration of Liquid Water Content (LWC) [25] from the base to the height of the 0°C isotherm.

$$VIL(K_{dp}) = \int_{0}^{h} 2,25 K_{dp}^{0,723} \cdot dh \tag{4}$$

Similarly, we calculated the ice content (Ice Water Content - IWC) for cases covered by polarimetric radars based on [26]) through Equation 5:

$$VII(K_{dp}, Z) = \int_{h_{-10°C}}^{h_{-40°C}} 0,71 K_{dp}^{0,65} Z^{0,28} \cdot dh \tag{5}$$

The VIL integrations in both equations were performed up to the height closest to the 0°C isotherm (obtained from the nearest sounding to each radar). Since the maximum column height will be below the freezing level, only liquid water is considered, excluding contributions from potential ice particles, as shown in [16]. The determined VIL and VII values were spatialized and saved separately from the original data in NetCDF format for each selected time interval. To visualize and carry out analyses, they are presented in the form of boxplots, allowing the assessment of different statistics concerning the obtained data.

2.4.3. CFADs

Utilizing the methodology proposed by [27], we examine the structure of clouds that generate intense rainfall. The analysis period selected is in line with the one used by [19]. In his case, it was utilized the moment when hail occurred at the surface as a reference point. He analyzed the 30 minutes before this moment and the 20 minutes after, totaling a 1-hour event. In the present study, the reference period used is PMAX. However, it is noteworthy that the rainfall may have happened at different

 doi:10.20944/preprints202404.0970.v1

instants within the analyzed period, unlike hail occurrences, which have a specific moment of the beginning of precipitation.

This phase of the study represents the final step associated with the verification/exclusion of cases. After selecting PMAX and the chosen period for analysis, missing data within the period and cases lacking sufficient duration for analysis were identified. It resulted in excluding several cases and finally arriving at the total number of selected events.

The CFADs are created similarly to the validation methodology, but we perform some preceding steps in this process, as illustrated in Figure 4. First, we apply a mask (step 1) to the VIL data using shapefiles outlining storm contours extracted from the tracker. Afterward, we locate the pixel with the highest VIL value (step 2) within the storm and create a 5x5 *km* area centered on this point (step 3). At this stage, we record the location (lat/lon) of this highest VIL point. In the next step (4), we use the data of the desired variable to construct the CFAD (in this study, we used reflectivity), and we add the previously created 5x5 *km* area at the same coordinate (lat/lon) as the recorded highest VIL point. Finally, we extract the vertical column, varying the data with respect to height (from 2 to 16 *km*), as exemplified in Step 5 of Figure 4. This process is carried out for each selected time step (from 30 minutes before PMAX to 20 minutes after). The CFAD methodology assesses the frequency of a specific height value. As the created area was 5x5 *km*, we acquired 25 reflectivity points for each height, resulting in 25 vertical profiles for each event.

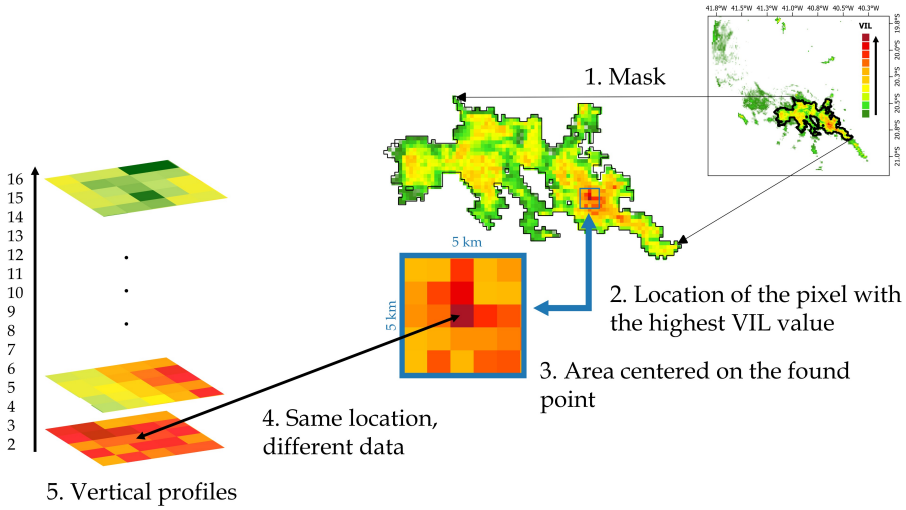

Figure 4. Procedure carried out to construct CFADs

Since the aim is to assess the structure of storms that occurred within a specific region, the CFAD is constructed by grouping all the events from that locality. For instance, we selected 17 events in the South region. Given that 25 vertical profiles are extracted for each event, the total number of profiles for the South region is calculated as $17 \times 25 = 425$. Consequently, the CFAD for the South region is built based on 425 vertical profiles.

2.5. Case Studies

We present three case studies to conduct a specific assessment regarding the microphysics of the selected events. The selected events occurred in the cities of Nova Alvorada do Sul (MS), Feira de Santana (BA), and Alfredo Chaves (ES), covered by the polarimetric radars of Jaraguari, Salvador, and Santa Teresa, respectively. These cases were chosen to study events in different locations. As polarimetric variables are analyzed to assess the microphysics of the events, regions covered only by conventional radars (South and North) are not included in this section. Vertical cuts are performed to evaluate the microphysical structure of the events using the polarimetric variables Differential Reflectivity (Z_{DR}), Specific Differential Phase (K_{DP}), and Cross-Correlation Coefficient (ρ_{HV}). The

 doi:10.20944/preprints202404.0970.v1

analyzed time period is the same as that used for generating CFADs, where, starting from the reference period (PMAX), 30 minutes before and 20 minutes after are examined, totaling 1 hour of the event.

Additionally, we present a fourth case study, conducting a microphysical analysis of events thar occured in the Southeast region of Brazil. We added this last case study to provide more information on the topic and to demonstrate the various possibilities of analyses that can be conducted in the future, as the study of intense rainfall events in the very short term is not sufficiently explored in the country. In this study, we calculated the CFADs for the reflectivity and Z_{DR} variables, as well as the life cycle of VIL and VII for the most intense pixel of each selected event. All calculations follow the same methodology discussed in this chapter.

3. Results and Discussion

3.1. Events

After completing thorough verification and validation processes, we identified 83 events, outlined in Table 2, and categorized by region.

Table 2. Number of events selected by region.

Region	Number of Events
South	17
Southeast	29
Midwest	14
North	15
Northeast	08

3.2. Regional Categorization

In this section we present the results obtained from calculating the water content (VIL), ice content (VII), and CFADs for the selected events. The analyses are conducted by comparing the differences between the selected events within the same region, juxtaposing them with other regions in the country. It is important to note that regional categorization serves as a means to group information, acknowledging that locations within the same region share similar (though not identical) characteristics concerning climate and typical meteorological events. Additionally, various factors, such as orography linked to storm structure and evolution [28,29], convection type, the system responsible for precipitation generation, and others, can influence these results. Nevertheless, despite these influencing factors, the study's primary objective is to discern any patterns in the behavior of the analyzed variables, disregarding differentiation among events and assuming they all contributed to intense rainfall.

3.3. VIL and VII

Figure 5 displays boxplots derived from the VIL calculations, organized by region, for each analyzed time frame. Initially, the South region (Figure 5 *e* exhibits the highest water content values, followed by the Midwest region (Figure 5 *c*, North region (Figure 5 *a*, Southeast region (Figure 5 *d*), and finally, the Northeast region (Figure 5 *b*). We established this hierarchy without taking into account the outlier values. The Southern and Central-West regions demonstrate similar behavior concerning medians (50th percentile, second quartile). The first 20 minutes of the event (at moments -30 minutes and -20 minutes) show lower medians, with values increasing at each subsequent time interval. Furthermore, we observed the highest median value at the -10 minute mark for both regions. This outcome suggests that the selected events in these regions experienced a rapid increase in water content from one moment to the next. Given that the median values remain high in the time intervals following PMAX, it is indicative that the rainfall may have persisted for several minutes throughout the cumulative period rather than occurring in just a few minutes. Additionally, some

 doi:10.20944/preprints202404.0970.v1

similar characteristics are noticeable among tropical regions (Figures 5 *a* and 5 *b*). The instants with the lowest median values are the first and last ones analyzed, respectively, and the highest values are concentrated between -20 minutes (-24 minutes, North region) and +10 minutes (+12 minutes, North region). Additionally, the moment featuring the highest median value is at -10 minutes (-12 minutes, North region). In contrast to the South and Midwest Regions, the VIL calculation for the North and Northeast regions shows both intensification and de-intensification of water content within the analyzed instants. In the first two regions, only VIL intensification is well-characterized. Therefore, it is suggested that the selected events in the North and Northeast regions may have had shorter durations compared to the South and Midwest. This information aligns with the findings of [30], where the authors report that rain cells belonging to typical cloud clusters in the Amazon (in both rainy and dry seasons) have a life cycle of 0.6 hours, indicating a short duration. Lastly, the Southeast region shows some similarity in the positioning of instants with higher and lower water content with the North region, concentrating the highest values between -20 minutes and PMAX. However, unlike the other regions, VIL extremes (outliers) are observed in almost every instant, which may be associated with the variability of the selected events, discussed later in Section 3.4

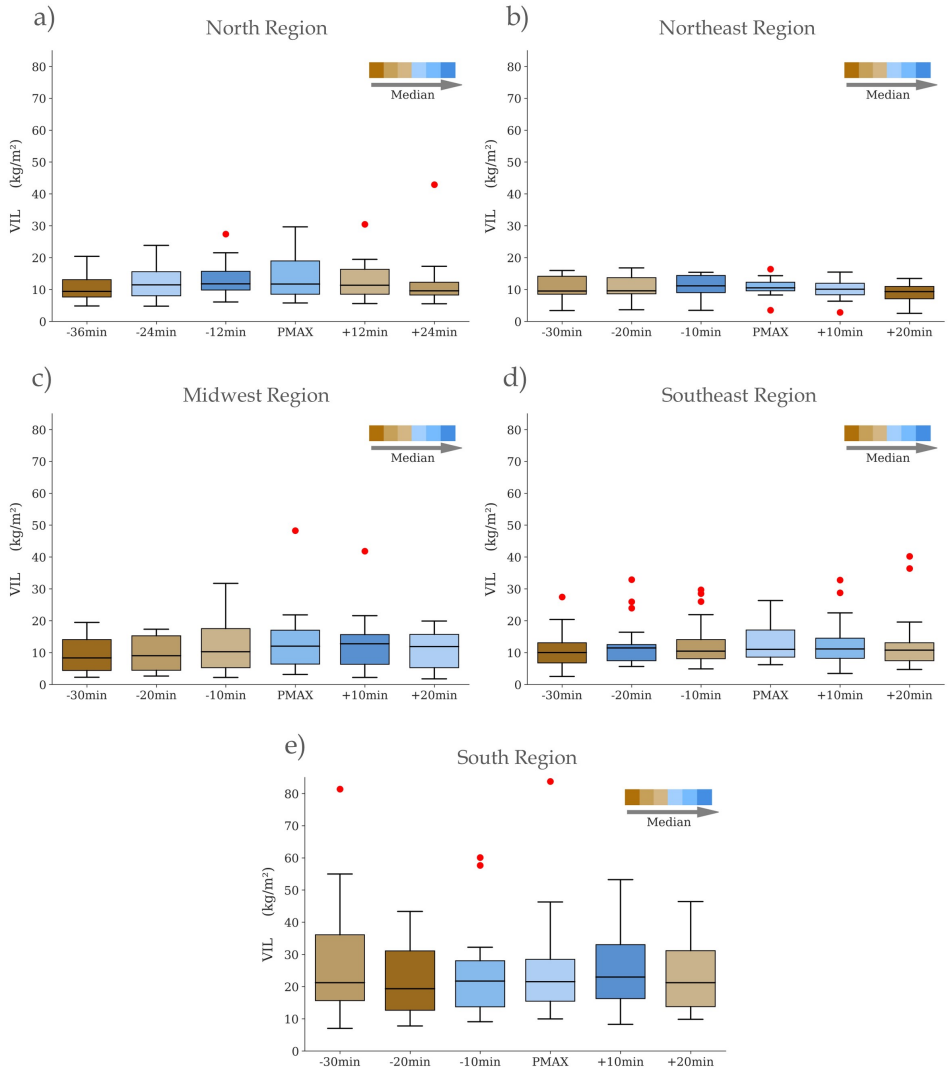

Figure 5. VIL calculation for the analyzed time instants. PMAX is the reference period for the highest reflectivity value over the station location during the event. The colors indicate the median values of the VIL values, with shades of blue referring to higher medians (higher VIL) and shades of brown for lower median values (lower VIL).

 doi:10.20944/preprints202404.0970.v1

While it is possible to infer certain information, as discussed above, uncertainties may be associated with them. One such uncertainty arises from the methodology of the VIL calculation, where we integrated water content up to the nearest height of the 0°C isotherm to account solely for the liquid water portion, as the VII, which considers the approximate ice layer, was also calculated. Since no differentiation was made regarding the type of system (deep or not) that generated the events, there is high variability in the types of clouds that may (or may not) have been considered. This variability may have influenced some results, especially in tropical regions where the formation of warm clouds is normal. Additionally, in the Northeast region, for instance, the analysis grouped VIL values calculated using both polarimetric and conventional radar equations, another factor that could influence the results. When examining the difference between the South and North regions, particularly questioning why North clouds exhibit lower VIL than the South clouds, given that the North region is warmer and should theoretically have clouds with a higher quantity of liquid water. Beyond the details mentioned above, this specific result may have been influenced by the fact that no calibration was performed between the used radars. As discussed in [31], Canguçu and Morro da Igreja radars (located in the Southern region) tend to slightly overestimate reflectivity values compared to the TRMM satellite radar, which was used as a reference. However, in the Northern region, [32] shows that the Belém and Manaus radars exhibit a high underestimation compared to the TRMM radar. In other words, the lack of radar calibration could have been a determining factor in the differences found between the Southern and Northern regions in the VIL calculation.

Figure 6 illustrates the calculation of ice content (VII) for the selected events. In general, we see a greater variability in the positions of the medians for the highest VII values is observed compared to the VIL values. Particularly concerning the regions of interest, the Southern region (Figure 6 *e*) exhibits notable disparities in ice content compared to other regions. Several studies consider the subtropical region of the South Atlantic (which includes the South brazilian region) as one of the areas on the planet most affected by severe convective events [33–37]. Such events involve clouds with deep vertical development, reaching very low temperatures, and consequently, they form a substantial amount of ice. Due to the presented values, Figure 6 *e* (related to the South region) uses a different scale compared to the others. We adjusted this to provide a clearer visualization of the results obtained among the regions.

In contrast to the South region, in the North region (Figure 6 *a*), there is minimal ice formation in the clouds. The North brazilian region is situated in the tropical region of the Earth, which is the part of the globe with the highest solar incidence, making it warmer [38]. Although the tropical region is also influenced by deep convection events [39,40], due to the higher temperatures, there is also the formation of warm clouds over the region, which practically do not produce ice.

The Midwest (Figure 6 *c*) and Southeast (Figure 6 *d*) regions exhibit outlier values in moments preceding PMAX, indicating that the studied clouds have ice peaks up to 30 minutes before PMAX occurs. Moreover, in the Midwest region, the highest median of VII values occurs immediately after PMAX, the exact moment with the highest VIL (Figure 5 *c*). Similarly, in the Northeast region (Figure 6 *b*), the highest median occurs at the moment just before PMAX, which is also the exact moment as the highest median for water content (Figure 5 *b*. Based on these results, we suggest that for the Northeast and Midwest regions, the onset of precipitation occurred around this moment. At that point, there was already sufficient water in the cloud to overcome gravity, and there was still ice present that could melt, sustaining intense precipitation for a longer duration.

Preprints.org (www.preprints.org) | NOT PEER-REVIEWED | Posted: 15 April 2024 doi:10.20944/preprints202404.0970.v1

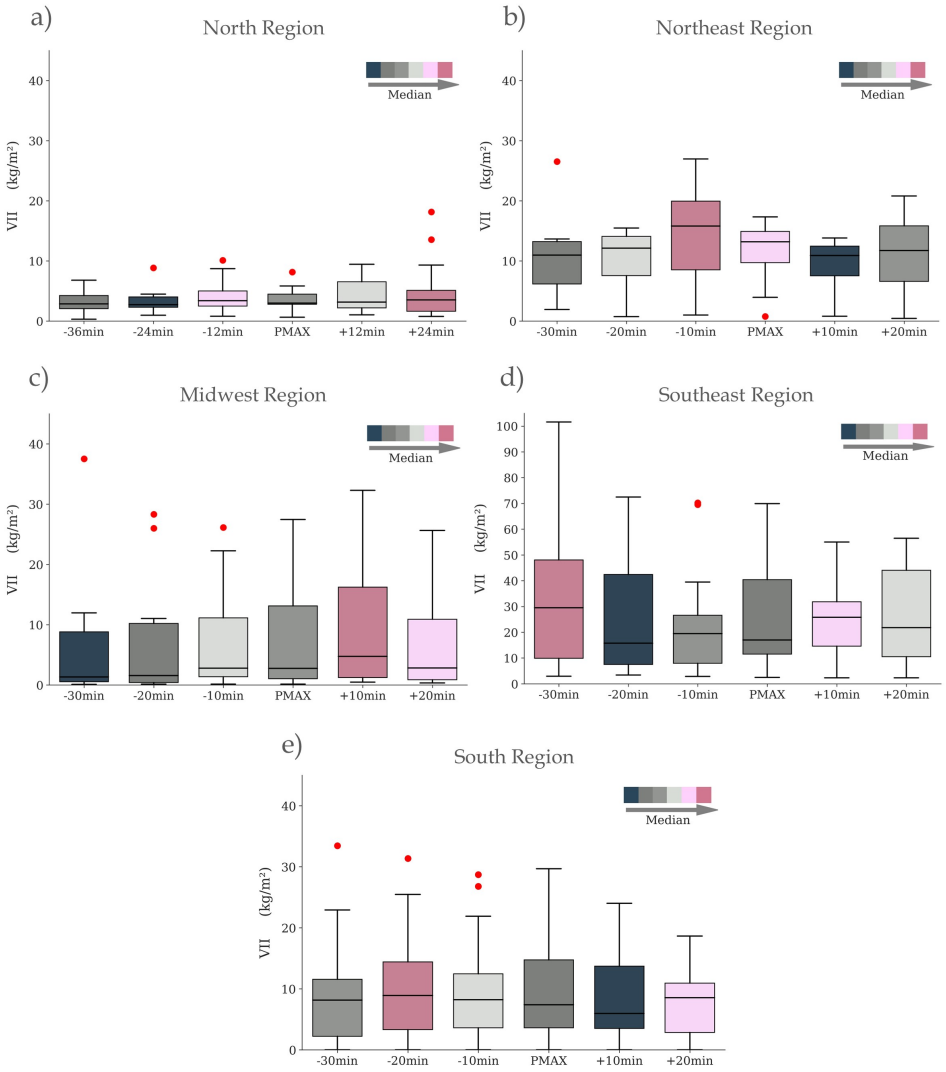

Figure 6. Similar to Figure 5, but for cloud-integrated ice content (VII).

3.4. CFADs

Constructing regional CFADs involves utilizing data from all selected radars, irrespective of their polarization. As conventional radars lack polarimetric variables, we cannot assess microphysical parameters across all events in this analysis. Therefore, we use only the reflectivity variable, which is common to both radar types.

Figure 7 displays the CFAD for the North region of Brazil, incorporating the 15 selected events in the area, constructed with 375 vertical profiles of clouds generating intense rainfall. In the figure, we observe an area with higher frequency values between the 40-45 dBZ and 50-55 dBZ intervals along the vertical axis for all analyzed time intervals. The reflectivity CFADs in this study are created using a 5x5 km sample (25 km^2) centered on the pixel with the highest VIL for each time interval of each studied event. As described in Section 2.4.2, we calculate VIL from liquid water content (LWC); that is, the pixel with the highest VIL used as the center of the sample is a region with high LWC. As discussed by [41], regions with high LWC values are closely associated with the location and intensity of updrafts in clouds. Therefore, we refer to the area with higher frequency values along the vertical axis as the updraft region. This association is also utilized by [19].

At the -36 minute mark in Figure 7, we observe the presence of an updraft, indicating that the clouds are already in the growth phase. Between -24 and -12 minutes before PMAX, there is a reduction in their height, but at -12 minutes, we observe a peak frequency in the 45-50 dBZ range, between

Preprints.org (www.preprints.org) | NOT PEER-REVIEWED | Posted: 15 April 2024 doi:10.20944/preprints202404.0970.v1

4 and 5 *km* in altitude. We suggest that this characteristic transition between -24 and -12 minutes is associated with the moment when the updraft is still transporting droplets to the higher parts of the cloud (-24 minutes). Shortly after, the process of collection and coalescence begins, making the droplets larger, and as they become heavier, they concentrate at lower altitudes (peak frequency at -12 minutes). At the PMAX moment, the updraft height increases again, reaching around 13 *km*, and we observe two peak frequencies, between 3 and 4 *km*, and between 5 and 6 *km*. This moment indicates that the cloud is still in the growth phase, being fed by the updraft. Since at -12 minutes there was already a higher concentration of droplets between 4 and 5 *km*, and the updraft at PMAX is still active, some of these droplets are again transported upward, while others concentrate in even lower regions of the clouds, generating the observed dual peaks. Finally, in the moments after PMAX, the peak frequencies progressively concentrate in the lower parts of the clouds, and the height of the most active part of the clouds decreases, indicating that they are entering the dissipation phase, and precipitation is already occurring. It is noteworthy that the PMAX period is merely a reference period, not necessarily associated with the onset of precipitation, as it may extend for several minutes throughout the cumulative period.

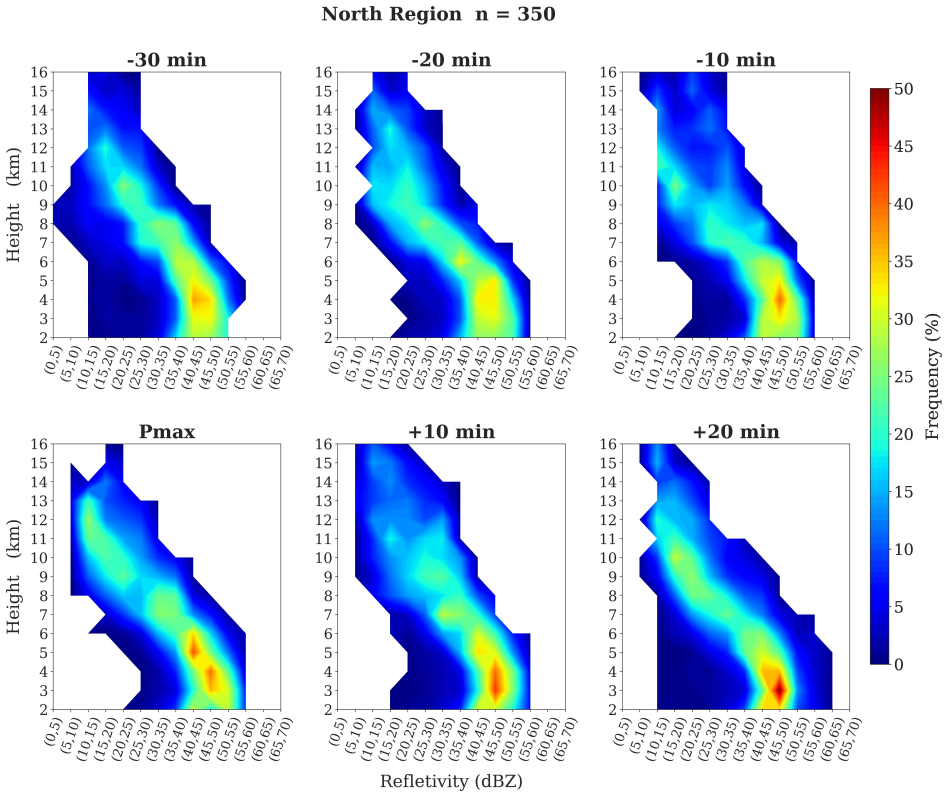

Figure 7. CFAD of the Northern region of Brazil created from an area 5 x 5 *km* (25 km^2), centered on the pixel with the highest VIL for 15 intense rain events selected in the region. n = 375 refers to the number of vertical profiles used in generating the CFAD. As 25 vertical profiles are extracted for each event (due to the size of the area) and 15 cases are studied in this region, there are a total of 375 vertical profiles to analyze the events as a whole.

Figure 8 presents the CFAD for the Northeast region of Brazil, constructed from 8 events, i.e., 200 vertical profiles. In the initial moment (-30 minutes), we observe that the updraft of the clouds is still in development, unlike the Northern region, where at -36 minutes, the clouds already have a formed updraft. Therefore, the events in the Northeast region exhibited a faster development than those in the North region. At -20 minutes, there is a strengthening of the updraft. At the moment just before PMAX (-10 minutes), frequency values around 35% are observed in the 45-50 dBZ range between 2 and 4 *km*, and the total height of the ascending air column is reduced. From this, we suggested that the

Preprints.org (www.preprints.org) | NOT PEER-REVIEWED | Posted: 15 April 2024 doi:10.20944/preprints202404.0970.v1

concentration of the highest frequency between 2 and 4 *km* is associated with the presence of raindrops that concentrate in the lower parts of the clouds, indicating that precipitation may have started around this moment. This information corroborates with the result from 5 *b*, where the median of the highest VIL value is at the same moment. In other words, considering all analyzed events in the Northeast region, it is the moment when the clouds have the highest amount of liquid water. At the PMAX moment, there is again a strengthening of the updraft, presenting frequency peaks, although not very intense, in higher regions of the clouds (between 9-10 *km* and 12-13 *km*), indicating the presence of ice. In 6 *b*, the moment with the highest amount of ice is also at -10 minutes, but as there might be a delay concerning reflectivity, and the data frequency is every 10 minutes, the presence of ice is more clearly observed at PMAX and not at -10 minutes. At +10 minutes, two frequency peaks are observed, between 6 and 7 *km* and between 8 and 9 *km*, which are associated with the weakening of the updraft, which is no longer strong enough to keep the ice in the higher parts of the clouds. Therefore, it starts to fall within the cloud, generating peaks at different heights. Finally, at the last moment, we observe reduced cloud activity as they are in the process of dissipation.

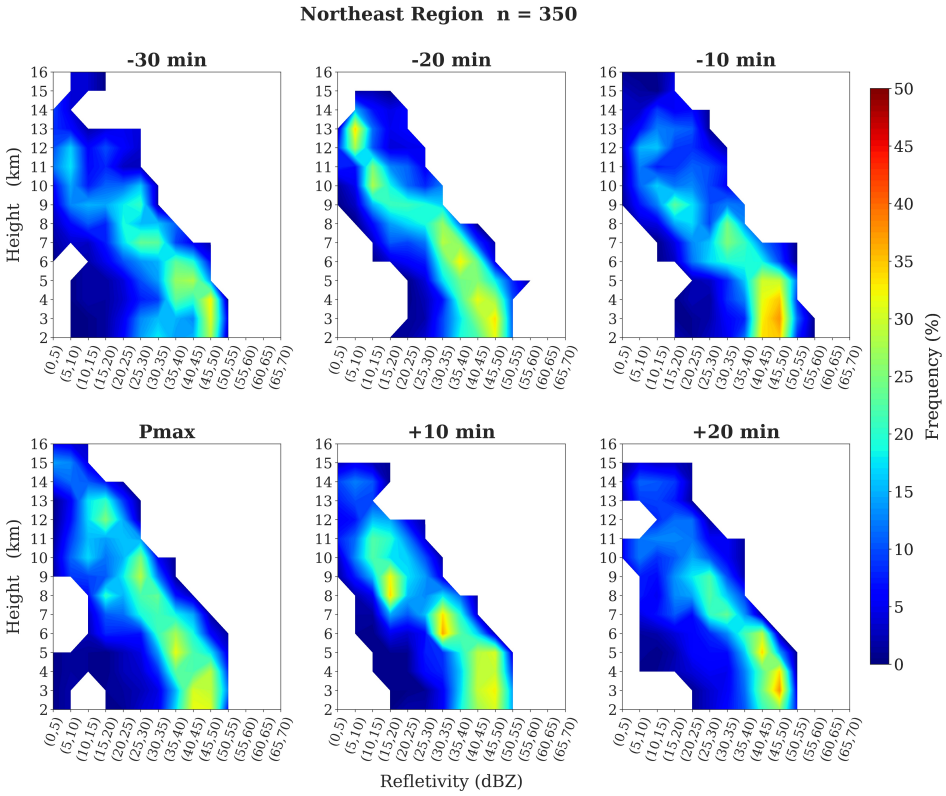

Figure 8. Similar to Figure 7 but for the Northeast region of Brazil. In total, 200 vertical profiles were used, referring to 08 selected events..

In Figures 9–11, corresponding to the CFADs of the Midwest, Southeast, and South regions, respectively, we observe outcomes with minimal frequency variability across the analyzed time intervals. To comprehend this characteristic, we calculate the standard deviation of reflectivity values to height for each moment of the analysis, as depicted in Figure 12. The 75th percentile value (9.95 dBZ) of the deviation data set is delimited by a vertical dashed line.

The South, Southeast, and Midwest regions (purple, red, green, respectively) emerge as the only areas where deviations surpass the 75th percentile (points to the right of the percentile line), specifically starting from a height of 5 *km* (horizontal dashed line). Additionally, the South region (purple) generally exhibits the highest deviation values among the three regions, followed by the Southeast, and lastly the Midwest. These findings align with their respective geographical characteristics. In contrast to tropical regions, areas at higher latitudes experience a more significant temperature gradient throughout

 doi:10.20944/preprints202404.0970.v1

the year and are more influenced by the Earth's rotation effects. These conditions contribute to a variety of phenomena, impacting overall precipitation in these regions. Due to the diverse range of events influencing these areas and generating distinct cloud structures, Figure 12 reveals that the most significant deviations are not localized in the lower parts of the clouds but occur above 5 *km* in height. Essentially, the intense rainfall events selected in the South, Southeast, and Midwest regions may have originated from clouds with both deep vertical development and shallower structures [42–44]. Notably, the Midwest, despite having tropical characteristics, is also affected by extratropical systems [45]. This characteristic becomes evident in Figure 12, where, despite showing high variability in the data, the Midwest region (among the three above the 75th percentile) exhibits the smallest deviations.

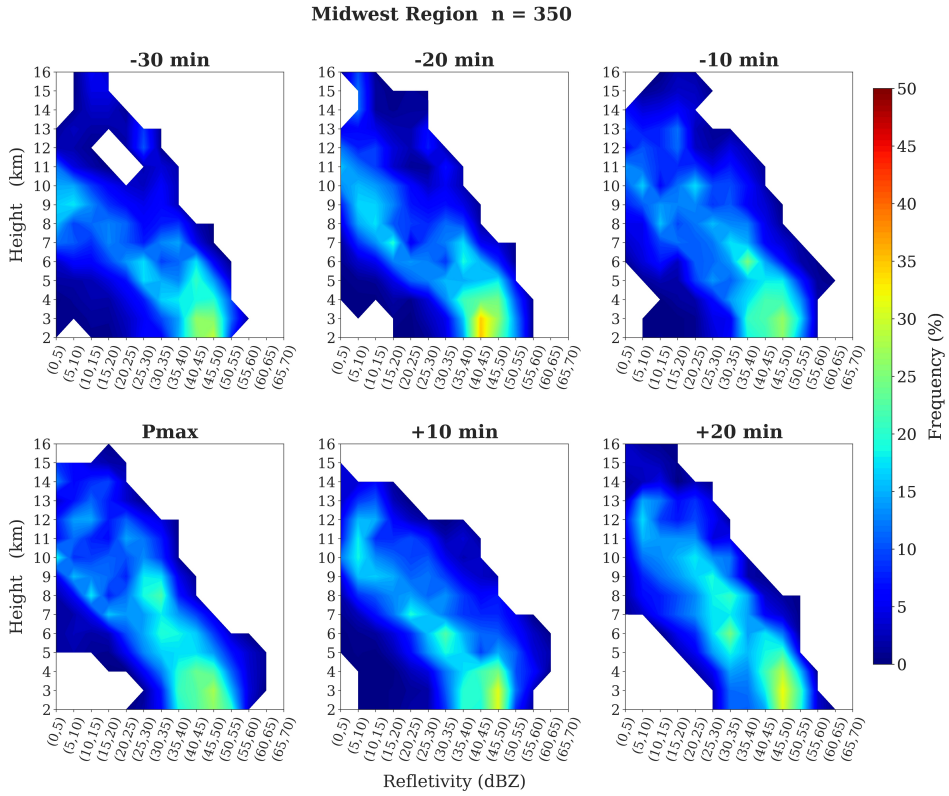

Figure 9. Similar to Figure 7 but for the Midwest region of Brazil. In total, 350 vertical profiles were used, referring to 08 selected events.

As this study does not differentiate between the systems responsible for generating events and the time of year in which they occur, the high variability of events in the South, Southeast, and Midwest regions is the factor behind the generation of CFADs with less pronounced results. Nevertheless, despite the CFAD in Figure 11 show high deviations in the dataset, some characteristics are observed. The first three moments do not exhibit significant frequency variations among them, but at the PMAX and +10 min moments, peaks of frequency in lower parts of the clouds are noticeable, suggesting a higher concentration of hydrometeors in those regions. Finally, at the +20 min moment, a weakening of the updraft is observed, already associated with the dissipation phase of the clouds.

 doi:10.20944/preprints202404.0970.v1

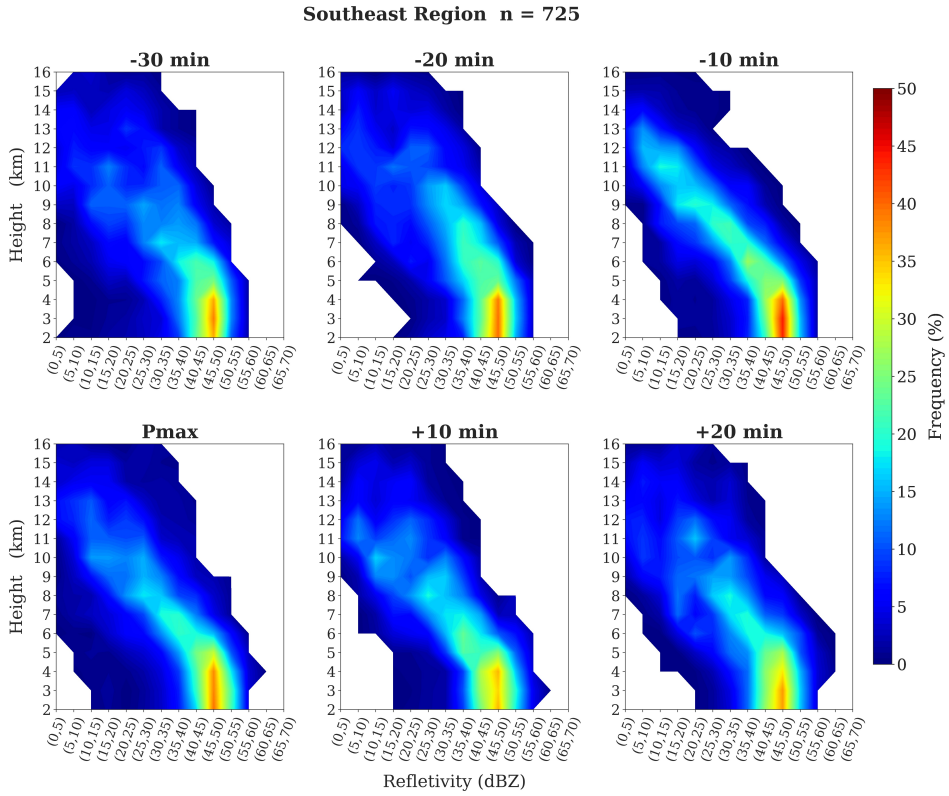

Figure 10. Similar to Figure 7 but for the Southeast region of Brazil. In total, 725 vertical profiles were used, referring to 08 selected events.

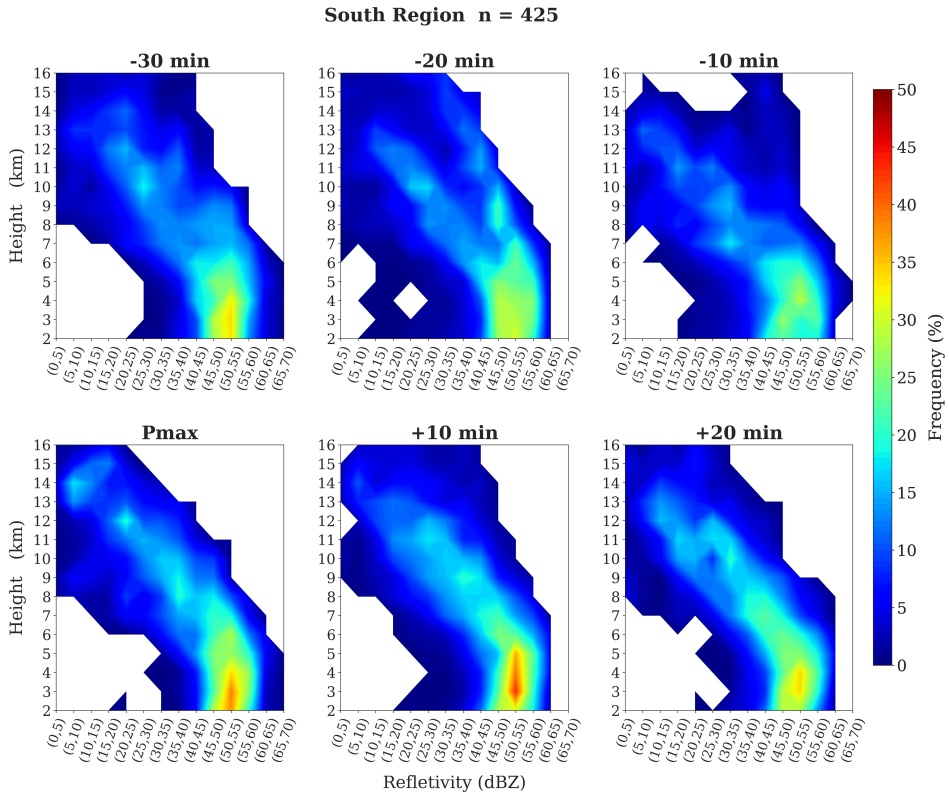

Figure 11. Similar to Figure 7 but for the South region of Brazil. In total, 425 vertical profiles were used, referring to 08 selected events.

Preprints.org (www.preprints.org) | NOT PEER-REVIEWED | Posted: 15 April 2024 doi:10.20944/preprints202404.0970.v1

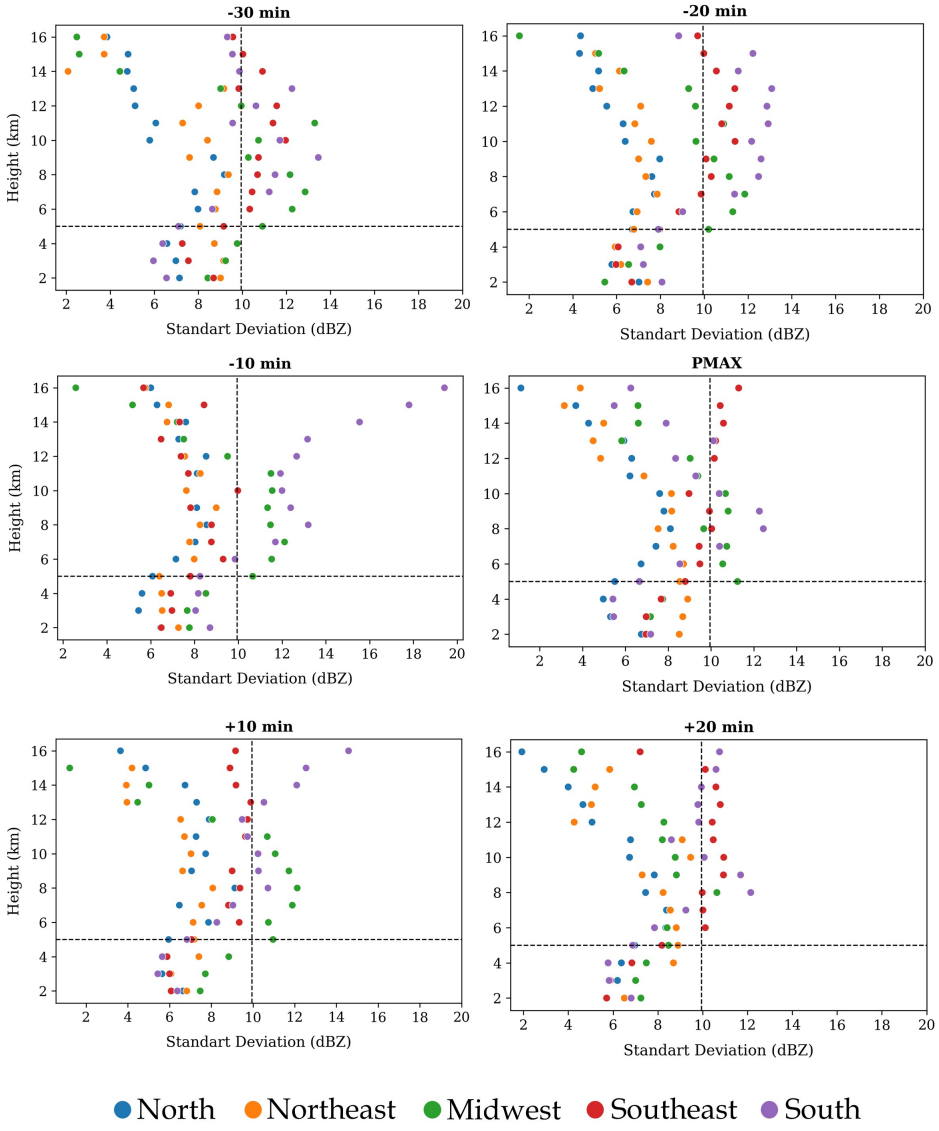

Figure 12. tandard deviations of reflectivity values as a function of height for each instant analyzed in the creation of the CFADS. The vertical line represents the 75th percentile (P75) of the entire deviation data set. The horizontal line represents the height at which the deviation values are above P75. The colors represent the deviations for each instant and height separated by regions.

Reflectivity serves as a variable for making associations and assumptions about the physical and morphological characteristics of hydrometeors. To obtain specific information, we need to use polarimetric variables since their values are directly linked to these characteristics. However, as the goal of this section is to analyze all regions of Brazil, and since not all regions are covered by polarimetric radars, we use reflectivity as the analytical variable. Although it is impossible to definitively determine the microphysical characteristics of hydrometeors present in the clouds, we can infer some information based on the literature. For example, clouds with intense vertical development typically reach very cold top temperatures as temperature decreases with height. [41] mention that if a cloud exceeds the height corresponding to 0°C, we can observe supercooled droplets. As the cloud reaches more negative temperatures, the presence of ice crystals, graupel, and hail becomes apparent. According to the authors, the probability of ice being present in a cloud with a top temperature of -13°C is 100%. Therefore, using this information and relying on the theory of warm and cold cloud formation, we can make some, albeit limited, associations with the microphysical processes that occur.

 doi:10.20944/preprints202404.0970.v1

3.5. Case Studies

In the previous section 3.4, the analysis of microphysics was not possible due to using data from radars with different polarizations to generate CFADs. To examine such characteristics, we conducted various case studies across the country. The following three case studies present selected events from each region of Brazil covered by polarimetric radars. Additionally, we introduce a fourth case study that focuses on a microphysical analysis of events occurring in the Southeast region of Brazil. We included this last case study to provide further insights into the topic and to showcase the diverse analytical possibilities for future investigations, considering that the study of intense short-term rainfall events is not sufficiently explored in the country.

3.5.1. Nova Alvorada do Sul (Jaraguari Radar)

This intense rainfall event occurred in the municipality of Nova Alvorada do Sul, located in the state of Mato Grosso do Sul, on February 5, 2020, between 17:00 and 18:00 UTC. During this event, 46.4 mm of rainfall was recorded within a one-hour period. At the station's location, the Jaraguari radar detected a maximum reflectivity of 51.75 dBZ at 3 km altitude at 17:24 UTC (PMAX). Figure 13 displays vertical cross-sections of polarimetric variables Z_{DR}, K_{DP}, and ρ_{HV}. These variables are commonly employed for the microphysical analysis of precipitation systems, as discussed in works such as [25,46,48–50], among others. The analysis moments range from -30 to +20 originally, adjusted due to the 12-minute radar data frequency from Jaraguari.

For a clearer understanding of the vertical cross-sections, Figure 13 *a* illustrates the location of each cut at different time instances, indicated by a black line. The cut is centered on the cloud region that reached its maximum reflectivity (PMAX) at the station. The north/northwest (south/southeast) edge corresponds to the left (right) side of Figures 13 *b*, *c*, *d*. It's noteworthy that at -36 minutes, the cloud is already formed with a reflectivity of around 40 dBZ. However, in the initial moment, various nuclei are observed close to each other, yet not highly organized. In subsequent timeframes, the system organizes itself, forming a larger convective area where points of reflectivity exceeding 50 dBZ (depicted in pink) are observed.

Z_{DR} is a variable directly linked to particle axis sizes. The more spherical the particles (droplets, hail), the closer Z_{DR} is to zero. Conversely, in the case of oblate hydrometeors (the horizontal axis is larger than the vertical, for example), Z_{DR} shows positive values. In the initial moments of Figure 13 *b*, at -36 minutes and -24 minutes, there are more intense Z_{DR} regions around 2 dB, between 2 and 4 km. These regions are observed at some points along the radar distance axis, but from the -12 minute mark, the more intense Z_{DR} values concentrate at distances greater than approximately 125 km. Furthermore, these Z_{DR} values extend vertically, with values around 3.5 dB up to 5 km altitude and approximately 2.5 dB between 5 and 10 km altitude. These regions, referred to as "Z_{DR} columns," are well-documented in the literature, as discussed by [47,48,51–53]. According to the authors, Z_{DR} columns are associated with the location and intensity of updrafts. Moreover, they may extend more than 3 km above the 0°C isotherm, indicating supercooled liquid droplets being lifted by the updraft from the cloud base to higher areas, creating this columnar appearance. Between the moments -24 min and -12 min, we see an increase in Z_{DR} values in the lower parts of the cloud, indicating the time when water droplets grow through microphysical processes of collision and coalescence and settle near the base due to their increased weight. Shortly after, at the PMAX moment, associated with the intensity of the updraft, these drops and droplets are lifted upwards and freeze. At the +12 min mark, negative Z_{DR} points are observed between 9 and 10 km altitude, indicating the freezing of the droplets. Due to the 12-minute interval between radar scans, some features may be missed during this time. Therefore, despite the indication of droplet freezing at this moment, it is suggested that freezing may have occurred in previous minutes, and at this specific moment, the ice within the cloud may already be melting, leading to the formation of more liquid water within the cloud. This suggestion is based on the observation that at this moment (+12 min), high Z_{DR} values are concentrated between 2 and 5

 doi:10.20944/preprints202404.0970.v1

km altitude. Finally, at the +24 min mark, these Z_{DR} values have already decreased, indicating that surface precipitation was already occurring between this time and the previous hour.

Some details mentioned in the Z_{DR} analysis are complemented by the results in Figure 13 *c*, which presents the values of the variable K_{DP}. As discussed in 3.4, K_{DP} is the specific differential phase. For spherical hydrometeors, there is no phase difference (or it is small) between the horizontal and vertical waves emitted by the radar, resulting in K_{DP} being close to zero. However, in the case of larger droplets with a more oblate shape, a phase difference is observed, leading to positive K_{DP} values. Various authors [54–58] also mention the presence of "K_{DP} columns" in clouds with deep convection, but these are typically spatially displaced to the west or northwest of the Z_{DR} column. We also observed such columns in this study from the -24 min moment. Between -24 min and -12 min, areas with positive K_{DP} values are still present at various points along the radar distance. However, from the PMAX moment onward, the K_{DP} column mainly concentrates between distances of 125 and 135 *km*, i.e., displaced northwest concerning the Z_{DR} columns, as reported in the literature. Additionally, at the PMAX moment, there is a notable presence of a negative K_{DP} core between 8 and 10 *km* altitude. This core aligns with the earlier suggestion in Figure 13 *b*, where a strengthening of the updraft is observed at the PMAX moment, leading to an increase in the height of the Z_{DR} column, indicating the transport of droplets and particles from the lower parts of the clouds to higher altitudes. These particles, reaching very cold temperatures, freeze through microphysical processes like aggregation and accretion. However, as reported by [47], despite the proximity of the Z_{DR} column to the K_{DP} column, the concentrations and types of hydrometeors present in the K_{DP} columns differ significantly. They are characterized by concentrations of small and medium-sized raindrops and melted ice particles (1-4 *mm*). Furthermore, K_{DP} columns are usually associated with the regions of cloud downdraft, unlike Z_{DR} columns. In other words, after the melting of the ice observed at the PMAX moment, there is an intensification of the downdraft, characterized by an increase in K_{DP} values at the +12 min moment. Therefore, from the analyses of the Z_{DR} and K_{DP} variables, it is concluded that precipitation began around the +12 min moment and extended for at least another 12 minutes, as positive K_{DP} values are still observed at the +24 min moment.

Finally, in Figure 13 *d*, we display the vertical cross-sections of the variable ρ_{HV}, which is linked to the particle heterogeneity. From the figure, we note values ranging between 0.8 and 0.9 at distances beyond approximately 130 *km* throughout the analyzed moments. As discussed by [47], lower values of ρ_{HV} are normally observed in the updraft region, where there may be the presence of hydrometeors with distinct shape and orientation characteristics.

 doi:10.20944/preprints202404.0970.v1

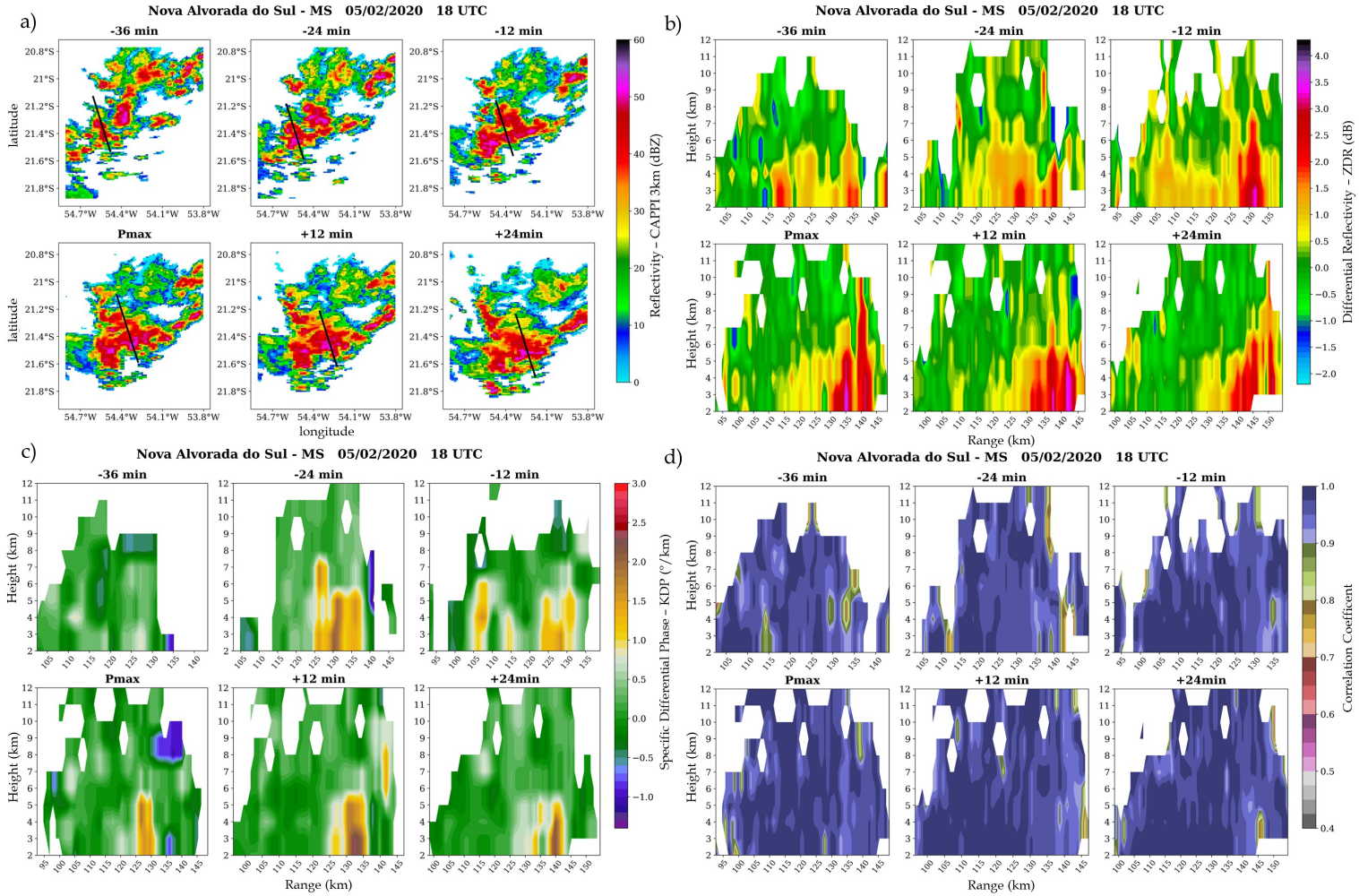

Figure 13. Vertical sections of the intense rain event in the municipality of Nova Alvorada do Sul - MS. a) Horizontal reflectivity in 3 *km* of the Jaraguari radar for the moments 36 minutes before and 24 minutes after the PMAX, totaling 1 hour. The black line indicates the location where the vertical cut is made. b) Vertical sections of the Z_{DR} variable for each instant analyzed. c) Vertical sections of the K_{DP} variable for each instant analyzed. d) Vertical sections of the variable ρ_{HV} for each instant analyzed. The x-axis of the vertical sections is oriented in the increasing direction of latitude.

 doi:10.20944/preprints202404.0970.v1

3.5.2. Feira de Santana (Salvador Radar)

The second case selected occurred in the municipality of Feira de Santana, Bahia, on January 23, 2020, at 21 UTC. Using reflectivity data from the Salvador radar, Figure 14 *a* illustrates that the system generating the event displays an extensive reflectivity area ranging between 35 and 50 dBZ throughout the analyzed moments. Consequently, it is a larger and different system compared to the first case study. This event accumulated 52.8 mm of rainfall in 1 hour, with the maximum reflectivity (on the 3 km CAPPI) observed over the station being 50.13 dBZ at 20:30 UTC (PMAX). The north/northwest (south/southeast) edges of the vertical cross-sections correspond to the left (right) side of Figures 14 *b*, *c*, *d*. In contrast to the first case study, from the initial analyzed moment (-30 min), the cloud appears in a more organized system, thus presenting some different microphysical characteristics. In Figure 14 *b*, we notice that at moments -30 min, -20 min, and -10 min, along the radar distance axis, there are various locations with positive Z_{DR} values, indicating that precipitation might have already been present, though perhaps not at its most intense. At the -10 min mark, values around 2.5 dB concentrate between distances of 110 and 115 km at altitudes of 2 to 4 km. As Z_{DR} values decrease in the subsequent time (PMAX), it is indicated that a more significant precipitation rate may have occurred between -10 min and PMAX. Comparing the moments in Figure14 *a*, it is noteworthy that there isn't a clear weakening of the system over the hours. Additionally, at the +10 min mark in Figure 14 *b*, some points of positive Z_{DR} are again observed in the lower parts of the clouds, indicating that precipitation may have persisted throughout the moments and not necessarily occurred in just a few minutes.

Figure 14 *c* shows that since the first moments, there are strong signs that precipitation was already present because the -20 min timeframe, in particular, exhibits the highest K_{DP} values in the lower parts of the cloud. An interesting detail emerges at the -10 min mark, where a core of negative K_{DP} values is observed between heights of 10 and 11 km, resembling the findings of the first case study despite different event origins. In both events, the core of negative K_{DP} values aligns with the higher Z_{DR} column, emphasizing that during the strengthening of the updraft, which transports droplets from the base to higher cloud regions, some of these droplets freeze. Subsequently, when this negative K_{DP} core is absent, new intensifications are observed at lower cloud levels in both K_{DP} and Z_{DR}. This suggests that the melting of this ice could serve as a robust indicator of increased surface precipitation. In Figure 14 *d*, it is evident that in the early moments (-30 min and -20 min), low ρ_{HV} values are distributed at various points along the vertical cut, not exceeding a height of approximately 4 km. However, at the -10 min mark, a core of ρ_{HV} values ranging between 0.8 and 0.9 is observed at heights of 5 to 7 km. This core is linked to the transport of droplets to higher cloud regions, resulting in the observation of different forms, orientations, and phases of hydrometeors at distinct heights, consistent with the findings at the same moment in Figures 14 *b* and *c*.

 doi:10.20944/preprints202404.0970.v1

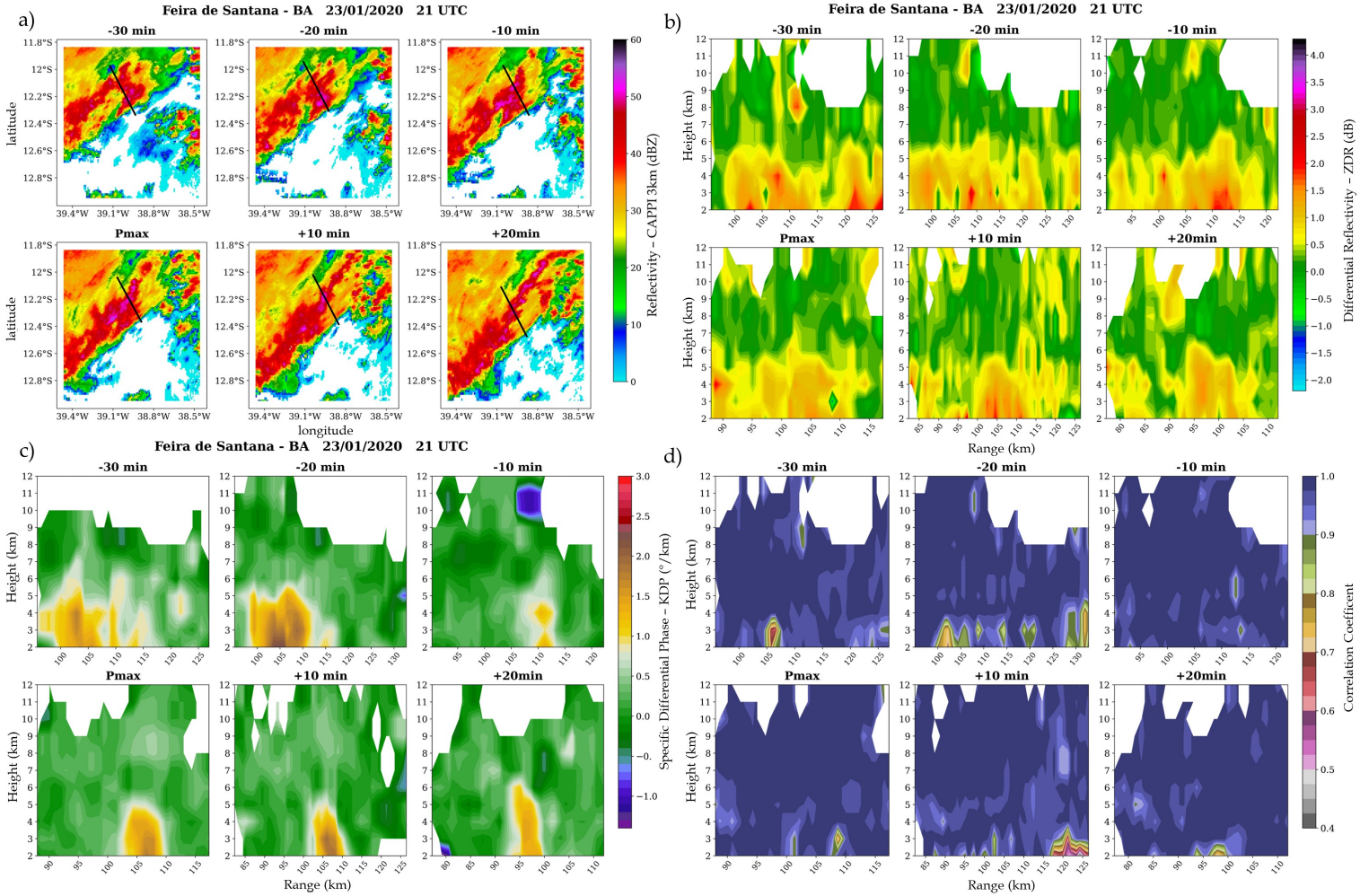

Figure 14. Similar to Figure 13, but for the case study of Feira de Santana - BA. The data comes from the Salvador radar.

 doi:10.20944/preprints202404.0970.v1

3.5.3. Alfredo Chaves (Santa Tereza Radar)

The third case study occurred in the municipality of Alfredo Chaves, in the state of Espírito Santo, on January 18, 2020 (January 17 in the local time), at 01 UTC. However, this event has a particularity: it consists of two selected cases. INMET stations recorded two intense rainfall events on January 18, one at 00 UTC, accumulating 51.2 mm, and another at 01 UTC, registering 51.6 mm. Interestingly, the PMAX times at the Alfredo Chaves station were at 23:50 (46.63 dBZ) in the first case and at 00 UTC (46.25 dBZ) in the second. In other words, despite the total accumulation being 102.8 mm in 2 hours, there is an indication that this precipitation may have occurred in a much shorter time frame, given the close PMAX registration times for both cases. Due to the substantial rainfall in a short period, it was chosen as the focus of the study. In Figure 15 *a*, it can be observed that, similarly to the second case study presented in this work, the cloud generating the event was already part of an organized system from the initial analyzed moment (-30 min). It already showed points with reflectivity greater than or equal to 50 dBZ. However, despite being already formed, it still intensifies over the moments, reaching its maximum over the station at the PMAX moment (using the 00 UTC PMAX in this case).

Figure 15 *b* reveals several points along the horizontal axis with Z_{DR} values ranging between 0.5 and 1.5 dB from 2 to 6 km in height. However, when comparing this figure with the Z_{DR} analyses from the two previous case studies, one can observe a lack of clear Z_{DR} columns. Instead, only a few isolated points of Z_{DR} between 1 and 2 dB are noted over the analyzed moments. At the -10 min moment, there is a subtle clustering of positive Z_{DR} values between distances of 70 and 75 km, potentially associated with a minor strengthening of the updraft in that region. As we progress through the moments in Figure 15 *c*, the K_{DP} column gradually establishes itself. At the PMAX moment, high K_{DP} values are observed in the lower parts of the clouds, linked to the descending current resulting from the precipitation within the cloud. In the subsequent moments, the column diminishes. An essential point to note is the presence of missing data in the Santa Tereza radar data from approximately 8 km in height. Consequently, despite not visualizing the formation of a negative K_{DP} core (associated with ice formation) before the intensification of the descending current, as seen in previous case studies, it is suspected that data gaps may have played a determining role in the non-visualization. This suspicion arises because, at +10 min and +20 min moments, cores of negative K_{DP} are still observed in the clouds. It is crucial to acknowledge that this is a hypothesis, as, unlike the other events, there is not a very significant increase in the observed updraft.

Finally, Figure 15 *d* displays the vertical cut with minimal variations in ρ_{HV}, indicating that there are not many hydrometeors with different shapes and orientations in the regions without data gaps. Therefore, for this specific study, the polarimetric variables primarily revealed the intensification of the descending current at the PMAX moment but did not provide many clues about why the intense rainfall event occurred. Consequently, it is suggested to develop different analyses to investigate the actual reasons for its occurrence, given that this event caused various disruptions for the population of Alfredo Chaves, as reported by [59].

 doi:10.20944/preprints202404.0970.v1

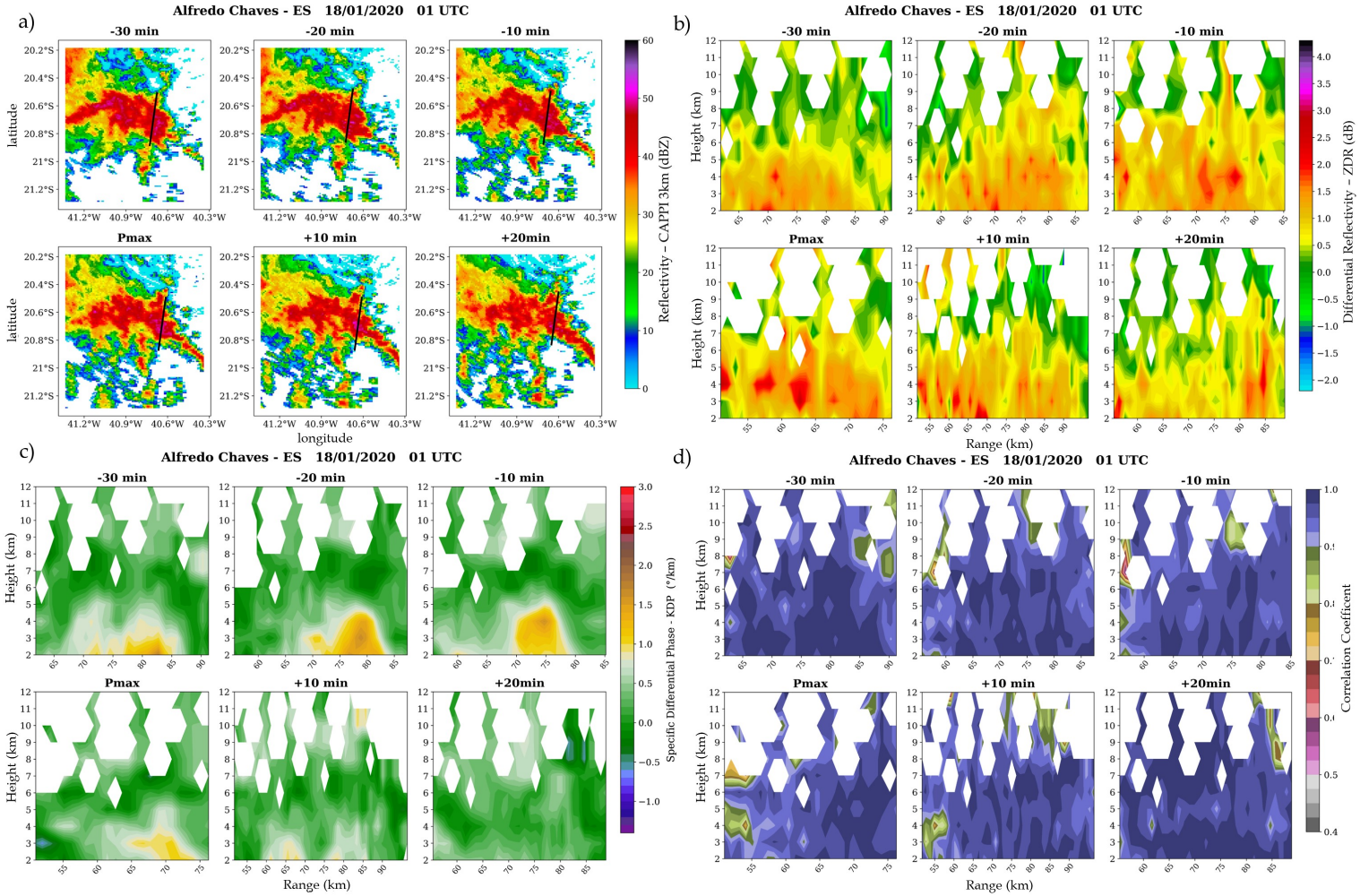

Figure 15. Similar to Figure 13, but for the case study of Alfredo Chaves - ES. The data comes from the Santa Teresa radar.

 doi:10.20944/preprints202404.0970.v1

3.5.4. Southeast Region

In this final case study, we present a different approach compared to the three events studied earlier. This difference arises from the aim of showcasing various types of analyses applicable to this type of event, especially when dealing with a topic that has received limited attention in local literature, as is the case with the subject of this work. Among the five regions examined in this study, the Southeast region exhibited the highest number of selected events covered by polarimetric radars. Therefore, it is chosen as the focus area for this case study. Figure 16 illustrates the locations of the radars used in this study, along with the automatic stations of INMET where the events were selected.

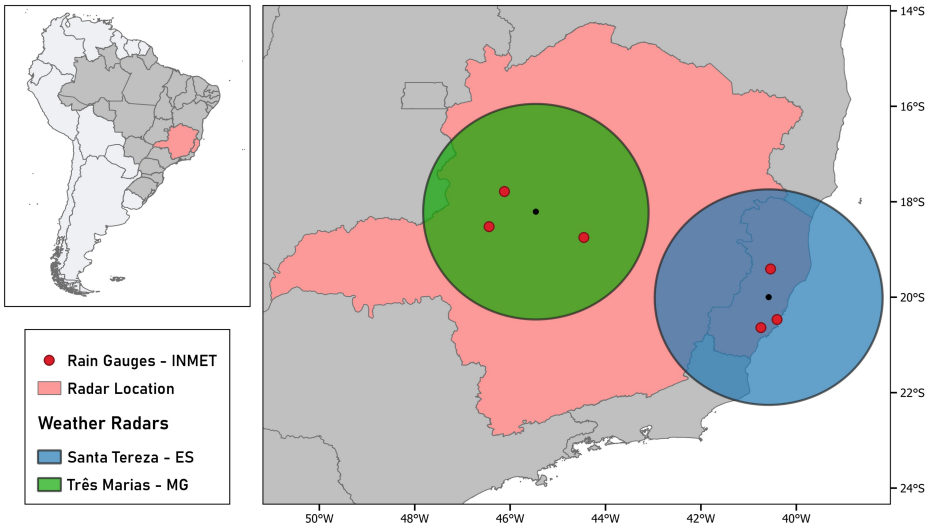

Figure 16. Location of the Santa Tereza (blue) and Três Marias (green) radars, and the INMET automatic stations (red) used in the study.

It is important to highlight that all criteria for selecting stations and events remain consistent with the overall methodology of this study. Furthermore, the same methodologies employed in the study for calculating integrated water (VIL) and ice (VII) content within clouds and constructing CFADs are also applied here. However, unlike Section 3.4, which exclusively examines the CFADs of reflectivity, this section includes an analysis of the CFAD for the Z_{DR} variable.

After applying all validation criteria, we selected seven intense rain events that accumulated more than 40 mm in 1 hour. Figure 17 presents the time series of VIL and VII calculations for the seven studied cases. Comparing the VIL and VII life cycles with radar reflectivity fields for each event (not shown), we observed some differences and similarities. As seen in Figures 17 a, b, e, and f, there is an increase in VIL and VII values just before the PMAX moment (dashed vertical line). Immediately after this increase, there is a sharp decrease in values. This suggests that the rise may be associated with convective development, where raindrops and ice particles grow in the cloud, resulting in high reflectivity values. As precipitation begins, VIL and VII values start to decrease. Despite these four events sharing a common characteristic (isolated developing cores), some nuances are notable. The events in Figures 17 a and b started their life cycle as small, isolated cores, reached maturity, and dissipated shortly after. However, the event in Figure 17 e showed an increase (mainly in ice content) but maintained high VIL and VII values for almost an hour before decreasing. Among the seven events studied, this was the one with the highest rainfall accumulation, exceeding 100 mm in 2 hours. As discussed in the previous case study analysis, there is an indication that this event generated rainfall in less than 2 hours, given the proximity of the PMAX times for both cases that compose this event. This information aligns with the VIL and VII life cycle since after 00 UTC, the values for both variables begin to reduce. In 17 f, there is an increase in VIL and VII minutes before the PMAX moment, followed by a decline. However, in subsequent instants, the life cycle shows a second peak in water and ice

 doi:10.20944/preprints202404.0970.v1

content. This feature is observed because, during the stage when the cloud is most intense, it splits into two cores, with the part responsible for the highest reflectivity reaching its peak and dissipating. On the other hand, the other core intensifies again, resulting in the second observed peak in VIL and VII values.

The events in Figures 17 *c* and *d* were cores belonging to larger-scale precipitating systems, so, in general, they did not show significant variations in the VIL and VII life cycles. However, the main difference between them is that the first (at a certain point) separated from the larger system and showed a peak of intensification.

Finally, and similarly to the previous ones, there are a few variations throughout the instances of the VIL and VII life cycle in the event in 17 *g*. This event was a small and localized core, which exhibited practically constant reflectivity values over the analyzed instances. Its peak of VIL and VII does not align with the PMAX moment, suggesting that the cloud responsible for the event generated rain more steadily over the 1-hour recording period.

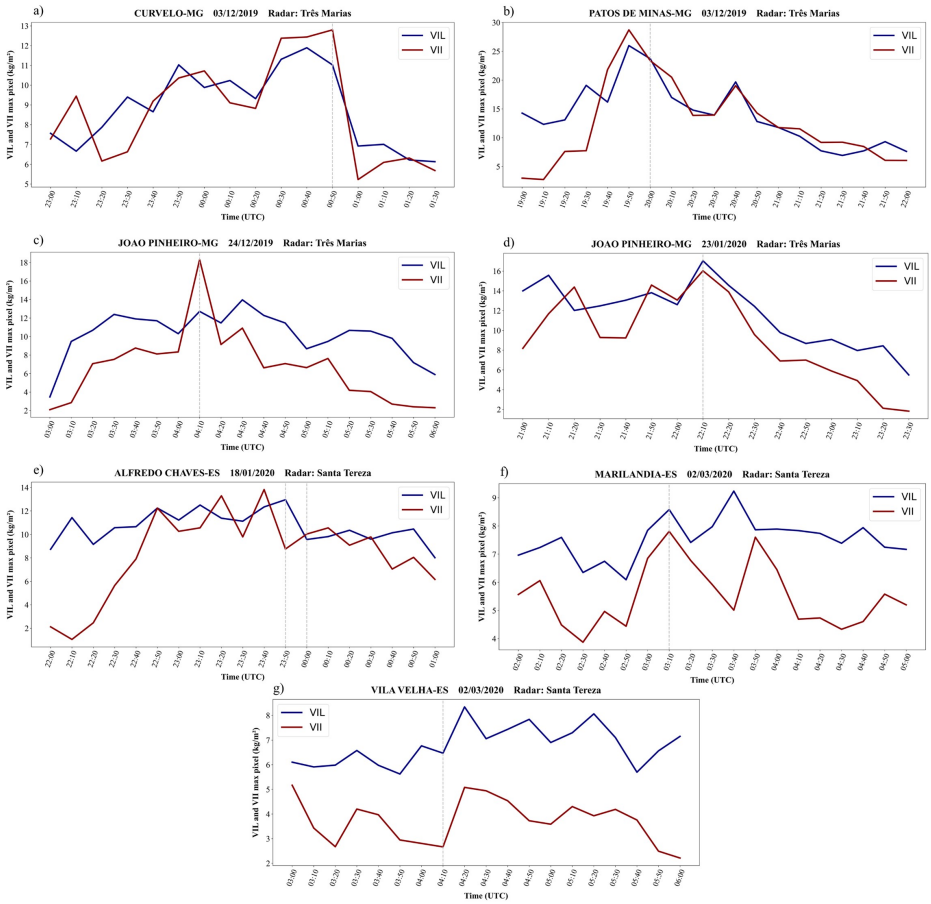

Figure 17. Life cycle of the water (VIL) and ice (VII) contents integrated in the cloud, in the highest intensity pixel (VIL and VII) of each analyzed event. The dashed vertical line indicates the PMAX instant.

In Figure 18 the CFAD of reflectivity for the seven selected cases is presented. Overall, there is no clear change in the vertical structure of the events over time. However, some characteristics stand out: the highest frequency values are observed between 45 - 50 dBZ, from the base up to approximately 4 km in height. At the -10 min moment, there is an increase in frequency values, suggesting a strengthening of the updraft and the presence of ice since PMAX is the instant of the highest reflectivity observed in the rain gauges, and the presence of ice in the clouds facilitates higher reflectivities. At the PMAX moment, the previously more structured column begins to decrease in height, possibly indicating

 doi:10.20944/preprints202404.0970.v1

the onset of precipitation. In the subsequent moments, there is no notable weakening of the clouds; therefore, it is suggested that the rain, in general, did not occur in a single moment but rather more continuously. [19] generated reflectivity CFADs for 16 hail events in the Southern region of Brazil. In contrast to the results obtained in this case study, the author found the formation of a more intense convective column, which quickly dissipated after hail started at the surface.

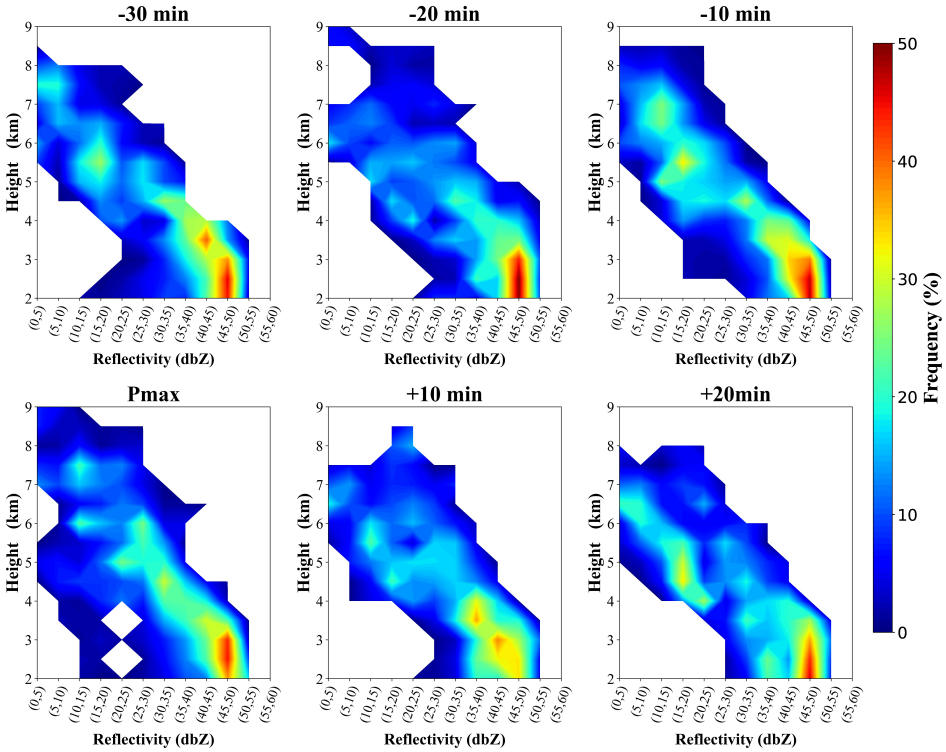

Figure 18. CFAD frequency diagram of the reflectivity variable using a 25 km^2 sample centered on the maximum VIL value for each instant analyzed. The CFAD was built from the 7 cases studied, and therefore, with 175 vertical profiles. PMAX is the reference period in which the maximum reflectivity value on the rain gauge was observed within the hour of recording the accumulated rainfall. The y-axis refers to height in km and the x-axis to reflectivity intervals in dBZ.

The calculation of the Z_{DR} variable CFAD is shown in Figure 19. At the -30 min and -20 min moments, the highest frequency values are between the 0 and 1 dB intervals, indicating the presence of spherical droplets in the lower parts of the clouds. Additionally, although low, there are frequency values between the 2.5 - 3 dB range, indicating that the clouds were in a growth phase. At the -10 min moment, the frequency values in the lower parts of the clouds decrease. In contrast, the convective column increases in height. This increase in the frequency of positive Z_{DR} values in higher parts of the clouds is associated with the Z_{DR} columns, also identified in previous case studies. Due to a strengthening of the updraft, drops, and droplets are transported to higher regions, which eventually freeze through processes like aggregation and accretion, resulting in a frequency peak in negative Z_{DR} intervals at an altitude of 8 km. At the PMAX moment, liquid drops fall within the cloud and grow through collision and coalescence processes, displaying the highest frequency values in the lower areas of the clouds. In the subsequent moments, frequency values decrease, but the column remains with a clear division of positive Z_{DR} values up to 6 km in height and negative values above this height. As the main column's weakening is not very evident, it is suggested, as highlighted in Figure 18, that the rain occurred continuously after the cloud initiated the precipitation process.

 doi:10.20944/preprints202404.0970.v1

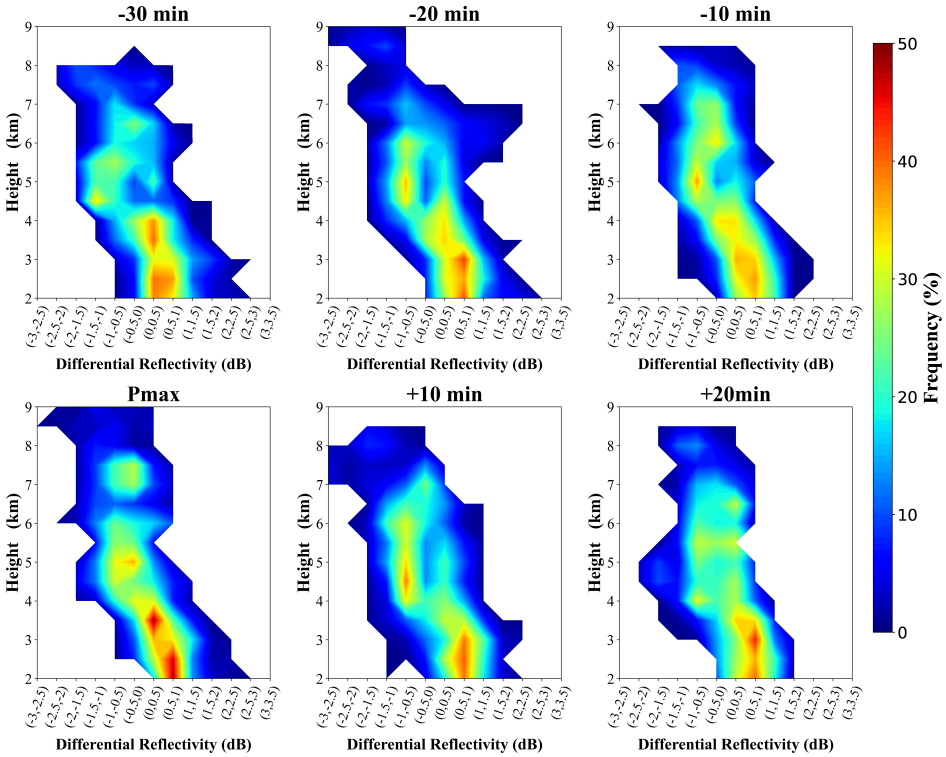

Figure 19. Similar to Figure 18, but for the Z_{DR} variable.

4. Conclusions

Despite the different techniques in the literature for defining intense rainfall in Brazil, many studies on the subject consider rainfall occurrence on a daily scale. However, numerous events associated with flash floods and rapid flooding occur over a short period. In Brazil, studies are scarce regarding sub-daily intense rainfall events, and existing studies focus on very specific regions. Therefore, the main objective of this study was to examine the structure and microphysical aspects associated with clouds generating intense rainfall over Brazil, resulting in high accumulations in a very short time (1h). Intense rainfall events were selected from hourly data from automatic rain gauges of the National Institute of Meteorology. After applying various validation criteria, 83 events were chosen and distributed across the five brazilian regions. The selected intense rainfall events exhibit the main convective column with reflectivity values ranging between 40 and 50 dBZ, generally extending to approximately 6 km in height in all regions of Brazil. Events in the Northeast region were faster compared to those in the North, as within the analyzed period, the North region already had formed clouds at the first analysis instant, while in the Northeast region, clouds were still developing. In the South, Southeast, and Midwest regions, reflectivity values did not show significant variations throughout the analyzed hours. However, the divergence of events considered in these regions was the factor responsible for the less expressive results, as each system can generate different cloud structures. This conclusion was drawn from calculating the standard deviations of events for each region, concerning height. From this calculation, we observed that the only regions where the deviations exceed the 75th percentile are these three regions. Additionally, the highest deviations are observed from 5 km in height, confirming the variability of the vertical structures of the events studied in these specific regions.

The VIL and VII life cycles show that events in the South region had the highest values among the regions throughout the analyzed moments. This result aligns with the fact that intense events that typically affect the region have a deep vertical development, reaching very low top temperatures, conducive to ice formation in clouds, often characterized as severe events. Events in the North and Northeast regions were faster than those in the Southern and Central-Western regions, as in the former, both intensification and de-intensification of VIL and VII values are observed, while in the latter, only

 doi:10.20944/preprints202404.0970.v1

the intensification of values is well evidenced. Regarding the case studies, it was found that the onset of intense precipitation in the events was preceded by a momentary intensification of the updraft, responsible for transporting drops and droplets to higher parts of the clouds. It is suggested that some of this content froze due to low temperatures, but in just 10 minutes, the melting of the particles was already observed in the studies, and there was an intensification in the downdraft, verified by the increase in values in the K_{DP} columns and the high frequency of positive Z_{DR} values in the lower parts of the clouds in the fourth case study. However, in the third case study, it was not possible to verify the Z_{DR} columns associated with the strengthening of the updraft in the moments before the intensification of the downdraft, nor the formation of ice in the higher parts of the cloud. However, various data gaps were observed in the Santa Tereza radar data from approximately 8 km in height, which also hindered the analysis of the event. Therefore, the development of other analyses in the future is suggested to verify the conditions that favored the occurrence of this event, as it caused significant damage to the municipality. Furthermore, the case study in the Southeast region showed that the selected events exhibited an abrupt increase in VIL and VII near the PMAX instant and then a drop when the events were isolated development cells. In contrast, when the events belonged to larger systems, there were not many variations in VIL and VII. From all the conducted analyses, it is concluded that short-term intense rainfall events are characterized by a rapid intensification of their structure, regardless of the region in Brazil. Additionally, the type of system responsible for generating the events significantly influences the results concerning the South, Southeast, and Midwest regions, as it becomes challenging to find certain patterns when there are various cloud structures. Therefore, it is suggested as a development for future work to conduct analyses of these events, making a separation of the synoptic (or mesoscale) system type responsible for generating them. Specifically evaluating events that occurred in different locations and generated by different systems, it is concluded that the momentary intensification of the updraft and subsequent melting are determining factors for the intensification of the downdraft and consequently the onset of intense precipitation. Because these characteristics occur within a few minutes, the predictability of the systems is complex, making it difficult to issue specific warnings promptly. Finally, it emphasizes the importance of continuing future studies aimed at evaluating the atmospheric conditions that determine short-term intense rainfall events.

Author Contributions: Conceptualization, Eliana Gatti, Izabelly Costa and Daniel Vila; Formal analysis, Eliana Gatti and Izabelly Costa; Methodology, Eliana Gatti; Software, Eliana Gatti; Supervision, Izabelly Costa and Daniel Vila; Writing – original draft, Eliana Gatti; Writing – review & editing, Izabelly Costa.

Funding: This research was funded by NATIONAL COUNCIL FOR SCIENTIFIC AND TECHNOLOGICAL DEVELOPMENT (CNPQ in Portuguese) during the first author's master's degree at the National Institute for Space Research.

Institutional Review Board Statement: Not applicable

Informed Consent Statement: Not applicable

Data Availability Statement: The data used in this work were made available by different public institutions and can be found through the links: https://bdmep.inmet.gov.br/; https://www.gov.br/cemaden/pt-br; https://www.gov.br/censipam/pt-br.

Acknowledgments: We would like to thank the institutions INMET, CEMADEN and SIPAM for providing data from radars and meteorological stations, which were essential for the development of the research.

Conflicts of Interest: The authors declare no conflicts of interest.

References

1. Alvares, C.A., et al. Köppen's climate classification map for Brazil. *Meteorologische Zeitschrift* **2013**, *22*, 711–728.
2. Brooks, H. E., Stensrud, D. J. Climatology of heavy rain events in the United States from hourly precipitation observations. *Monthly Weather Review* **2000**, *4*, 1194–1201.

 doi:10.20944/preprints202404.0970.v1

3. Konrad, C. E. Synoptic-scale features associated with warm season heavy rainfall over the interior southeastern United States. *Weather and Forecasting* **1997**, *12*, 557–571.
4. Groisman, P. Y., Knight, R. W., Karl, T. R. Changes in intense precipitation over the central United States. *Journal of Hydrometeorology* **2012**, *13*, 47–66.
5. Dolif, G., Nobre, C. Improving extreme precipitation forecasts in Rio de Janeiro, Brazil: are synoptic patterns efficient for distinguishing ordinary from heavy rainfall episodes? *Atmospheric Science Letters* **2012**, *13*, 216–222.
6. Teixeira, M. S., Satyamurty, P. Dynamical and synoptic characteristics of heavy rainfall episodes in southern Brazil. *Atmospheric Science Letters* **2007**, *135*, 598–617.
7. Liebmann, B., Jones, C., de Carvalho, L. M. Interannual variability of daily extreme precipitation events in the state of Sao Paulo, Brazil. *Journal of Climate* **2001**, *14*, 208–218.
8. Carvalho, L. M., Jones, C., Liebmann, B. Extreme precipitation events in southeastern South America and large-scale convective patterns in the South Atlantic convergence zone. *Journal of Climate* **2002**, *15*, 2377–2394.
9. Groisman, P. Y., Knight, R. W., & Karl, T. R. Heavy precipitation and high streamflow in the contiguous United States: Trends in the twentieth century. *Bulletin of the American Meteorological Society* **2001**, *82*, 219–246.
10. Lima, K. C., Satyamurty, P., & Fernández, J. P. R. Large-scale atmospheric conditions associated with heavy rainfall episodes in Southeast Brazil. *Theoretical and Applied Climatology* **2010**, *101*, 219–246.
11. Pristo, M. V. D. J., Dereczynski, C. P., Souza, P. R. D., & Menezes, W. F. Climatologia de Chuvas Intensas no Município do Rio de Janeiro. *Revista Brasileira de Meteorologia* **2018**, *33*, 615–630.
12. Murphy, A. M., Ryzhkov, A., & Zhang, P. Columnar vertical profile (CVP) methodology for validating polarimetric radar retrievals in ice using in situ aircraft measurements. *Journal of Atmospheric and Oceanic Technologya* **2020**, *37*, 1623–1642.
13. Murphy, A. M., Ryzhkov, A., & Zhang, P. Recent progress in dual-polarization radar research and applications in China. *Advances in Atmospheric Sciences* **2019**, *36*, 961–974.
14. Queiroz, A. P. Monitoramento e Previsão Imediata de Tempestades Severas usando dados de Radar. Master Dissertation, National Institute for Space Research, São José dos Campos-SP, 2009.
15. Uba, D. M. TATHU - Software para rastreio e análise do ciclo de vida de sistemas convectivos. National Institute for Space Research, São José dos Campos-SP, 2022.
16. Cecchini, M. A., Silva D., Maria A. F., Machado, L.A.T., Morales R., Carlos A., Biscaro, T. Macrophysical and microphysical characteristics of convective rain cells observed during SOS-CHUVA. *Journal of Geophysical Research: Atmospheres* **2020**, *125*, e2019JD031187.
17. Greene, D. R., Clark, R. A. Vertically integrated liquid water—A new analysis tool. *Monthly Weather Review* **2019**, *100*, 548–552.
18. Carey, L. D., Rutledge, S. A. The relationship between precipitation and lightning in tropical island convection: A C-band polarimetric radar study. *Monthly Weather Review* **2020**, *128*, 2687–2710.
19. Sperling, V. B. Processos Físicos e Elétricos das Tempestades de Granizo na Região Sul do Brasil. Doctoral Thesis, National Institute for Space Research, São José dos Campos-SP, 2009.
20. Sachidananda, M. and Zrnić, D.S. Rain rate estimates from differential polarization measurements. *Journal of Atmospheric and Oceanic Technology* **1987**, *4*, 588–598.
21. Zrnić, D.S., Ryzhkov, A. Advantages of rain measurements using specific differential phase. *Journal of Atmospheric and Oceanic Technology* **1996**, *13*, 454–464.
22. Ryzhkov, A. V., Giangrande, S. E., Schuur, T. J. Rainfall estimation with a polarimetric prototype of WSR-88D. *Journal of Applied Meteorology* **2005**, *44*, 502–515.
23. Giangrande, S. E., Ryzhkov, A. V. Estimation of rainfall based on the results of polarimetric echo classification. *Journal of applied meteorology and climatology* **2008**, *47*, 2445–2462.
24. Thompson, E. J., Rutledge, S. A., Dolan, B., Thurai, M., Chandrasekar, V. Dual-polarization radar rainfall estimation over tropical oceans. *Journal of applied meteorology and climatology* **2018**, *57*, 755–775.
25. Ryzhkov, A. V., Zrnic, D. S. The title of the cited contribution. In *Radar polarimetry for weather observations*; Cham, Switzerland: Springer International Publishing, 2019.
26. Bukovčić, P. and Ryzhkov, A., Zrnić, D., Zhang, G. Polarimetric radar relations for quantification of snow based on disdrometer data. *Journal of Applied Meteorology and Climatology* **2018**, *57*, 103–120.

 doi:10.20944/preprints202404.0970.v1

27. Yuter, S. E., Houze, R. A. Three-dimensional kinematic and microphysical evolution of Florida cumulonimbus. Part II: Frequency distributions of vertical velocity, reflectivity, and differential reflectivity. *Monthly weather review* **2018**, *123*, 1941–1963.
28. Markowski, P. M., Dotzek, N. A numerical study of the effects of orography on supercells. *Atmospheric research* **2011**, *100*, 457–478.
29. Houze Jr, Robert A. Orographic effects on precipitating clouds. *Reviews of Geophysics* **2012**, *50*.
30. Machado, L. A. T., Calheiros, A. J. P., Biscaro, T., Giangrande, S., Silva Dias, M. A.F., Cecchini, M. A., Albrecht, R., Andreae, M. O., Araujo, W. F. and Artaxo, P., et. al. *Atmospheric Chemistry and Physics* **2018**, *18*, 6461–6482.
31. Costa, I.C. Avaliação dos dados produzidos pela rede de radares meteorológicos de banda "S" localizados no centro sul do Brasil. Master of Science Thesis [in Portuguese], National Institute for Space Research, São José dos Campos-SP, 2007.
32. Saraiva, I. ariabilidade regional das nuvens de chuva na Bacia Amazônica visto por uma rede de radares meteorológicos. Doctoral Thesis, National Institute for Amazon Research, Manaus-AM, 2016.
33. Fujita, T. T. Tornadoes around the world. *Weatherwise* **1973**, *26*, 56–83.
34. Silva Dias, M. A. F. Editor 1, R. Pielke Sr., Editor 2, R. Pielke Jr., Eds., Vol II. 1999.
35. Nascimento, E. L. Previsão de tempestades severas utilizando-se parâmetros convectivos e modelos de mesoescala: uma estratégia operacional adotável no Brasil. *Revista Brasileira de Meteorologia* **2005**, *20*, 121–140.
36. Brooks, H.E. A global view of severe thunderstorms: Estimating the current distribution and possible future changes, Preprints. In Proceedings of AMS Severe Local Storms Special Symposium Atlanta, 2006.
37. Zipser, E. J., Cecil, D. J., Liu, C., Nesbitt, S. W., Yorty, D. P. Where are the most intense thunderstorms on Earth? *Bulletin of the American Meteorological Society* **2006**, *87*, 1057–1072.
38. Stevens, A. P. Introduction to the basic drivers of climate. **2010**
39. Krishnamurti, T. N., Stefanova, L., Misra, V. *Tropical meteorology*, 1979.
40. Hastenrath, S. Climate dynamics of the tropics. *Springer Science & Business Media* **2012**, *8*, 1057–1072.
41. Wallace, J., Hobbs, P. V. In *Atmospheric science: an introductory survey*; Elsevier; 2006;
42. Sohn, B. J. et al. Characteristic features of warm-type rain producing heavy rainfall over the Korean Peninsula inferred from TRMM measurements. *Monthly Weather Review* **2013**, *141*, 3873–3888.
43. Song, H. J. et al. Idealized numerical experiments on the microphysical evolution of warm-type heavy rainfall. *Journal of Geophysical Research: Atmospheres* **2017**, *122*, 1685–1699.
44. Sohn, B. J., Ryu, G. H., Song, H. J. Observational Characteristics of Warm-Type Heavy Rainfall. *Satellite Precipitation Measurement* **2020**, 745–759.
45. INPE. Observational Characteristics of Warm-Type Heavy Rainfall. *Climanálise* **1986**.
46. Kumjian, M. R. Principles and Applications of Dual-Polarization Weather Radar. *Journal of Operational Meteorology* **2013a**, *1*.
47. Kumjian, M. R. Principles and Applications of Dual-Polarization Weather Radar. Part II: Warm-and Cold-Season Applications. *Journal of Operational Meteorology* **2013b**, *1*.
48. Kumjian, M. R., et. al. The anatomy and physics of Z DR columns: Investigating a polarimetric radar signature with a spectral bin microphysical model. *Journal of Applied Meteorology and Climatology* **2014**, *53*, 1820–1843.
49. Tobin, D. M., Kumjian, M. R. Microphysical and polarimetric radar modeling of hydrometeor refreezing. *Journal of the Atmospheric Sciences* **2021**, *78*, 1965–1981.
50. Segall, J. H., French, M. M., Kingfield, D. M., Loeffler, S. D, Kumjian, M. R. Storm-scale polarimetric radar signatures associated with tornado dissipation in supercells. *Weather and Forecasting* **2022**, *37*, 3–21.
51. Picca, J. C.; Kumjian, M. R.; Ryzhkov, A. V. Z_{DR} columns as a predictive tool for hail growth and storm evolution. In Proceedings of 25th Conf. on Severe Local Storms, 2010
52. Dalman, D. M. et al. Cataloging rapid-scan observations of Z DR columns in supercells. In Proceedings of 29th Conference on Severe Local Storms, Stowe, VT, USA, 2018.
53. Picca, J. C.; Snyder, J. C. and Ryzhkov, A.V. An observational analysis of Z_{DR} column trends in tornadic supercells. In Proceedings of 37th Conf. on Radar Meteorology, Norman, OK, Amer. Meteor. Soc., 5A. 5, 2015
54. Ryzhkov, A. V.; Schuur, T. J.; Burgess, D. W.; Zrnic, D. S. Polarimetric tornado detection. *Journal of applied meteorology* **2005**, *44*, 557–570.

 doi:10.20944/preprints202404.0970.v1

55. Kumjian, M. R.; Ryzhkov, A. V. Polarimetric signatures in supercell thunderstorms. *Journal of applied meteorology and climatology* **2008**, *47*, 1940–1961.
56. Romine, G. S.; Burgess, D. W.; Wilhelmson, R. B. A dual-polarization-radar-based assessment of the 8 May 2003 Oklahoma City area tornadic supercell. *Journal of applied meteorology and climatology* **2008**, *136*, 2849–2870.
57. Kumjian, M. R.; Ryzhkov, A. V.; Melnikov, V. M.; Schuur, T. J.; Rapid-scan super-resolution observations of a cyclic supercell with a dual-polarization WSR-88D. *Monthly weather review* **2010**, *138*, 3762–3786.
58. Snyder, J. C. and Bluestein, H. B.; Venkatesh, V.; Frasier, S. J; Observations of polarimetric signatures in supercells by an X-band mobile Doppler radar. *Monthly weather review* **2013**, *141*, 3–29.
59. Tribuna Online. Available online: https://tribunaonline.com.br/previsaodotempo/alfredo-chaves-e-a-cidade-que-recebeu-mais-chuva-em-janeiro-no-brasil-diz-instituto-60662 (accessed on 20 May 2022).
60. Villarini, G.; Krajewski, W. F. Review of the different sources of uncertainty in single polarization radar-based estimates of rainfall. *Surveys in Geophysics* **2010**, *31*, 107–129.